AD-A157 937 AUGA2 ON GASB(001): AN EPITAXIAL THERMODYNAMICALLY STABILIZED METAL/III-V.. (U) CALIFORNIA UNIV LOS ANGELES DEPT OF CHEMISTRY AND BIOCHEMISTR.. J R LINCE ET AL. 1/1

UNCLASSIFIED AUG 85 TR-7 N00014-83-K-0612 F/G 20/12 NL

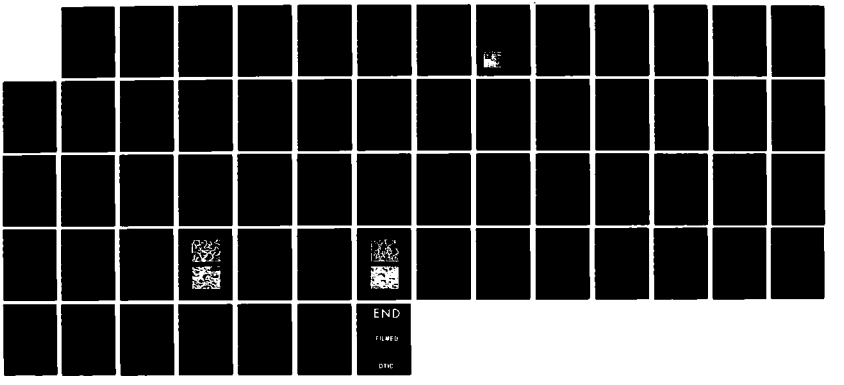

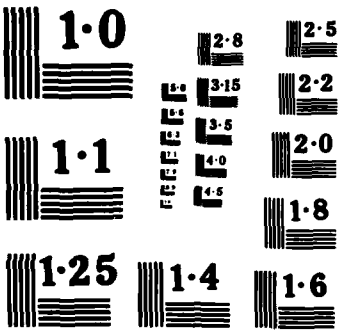

NATIONAL BUREAU OF STANDARDS
MICROCOPY RESOLUTION TEST CHART

OFFICE OF NAVAL RESEARCH

Research Contract N00014-83-K-0612

TECHNICAL REPORT No. 7

$AuGa_2$ ON GaSb(001): AN EPITAXIAL, THERMODYNAMICALLY STABILIZED METAL/III-V COMPOUND SEMICONDUCTOR INTERFACE

by

Jeffrey R. Lince and R. Stanley Williams

To Be Published

in

J.Vac.Sci.Techol. B 3 (1985)

Department of Chemistry and Biochemistry
University of California, Los Angeles, CA 90024

August, 1985

UNCLASSIFIED

SECURITY CLASSIFICATION OF THIS PAGE (When Data Entered)

REPORT DOCUMENTATION PAGE	READ INSTRUCTIONS BEFORE COMPLETING FORM
1. REPORT NUMBER: 7	2. GOVT ACCESSION NO.: AD-A157937
3. RECIPIENT'S CATALOG NUMBER	
4. TITLE (and Subtitle): $AuGa_2$ on GaSb(001): An epitaxial, thermodynamically stabilized metal/III-V compound semiconductor interface	5. TYPE OF REPORT & PERIOD COVERED: Technical Report - Dec 84 - Aug 85
	6. PERFORMING ORG. REPORT NUMBER
7. AUTHOR(s): Jeffrey R. Lince and R. Stanley Williams	8. CONTRACT OR GRANT NUMBER(s): N00014-83-K-0612
9. PERFORMING ORGANIZATION NAME AND ADDRESS: Department of Chemistry & Biochemistry, UCLA, Los Angeles, CA 90024	10. PROGRAM ELEMENT, PROJECT, TASK AREA & WORK UNIT NUMBERS
11. CONTROLLING OFFICE NAME AND ADDRESS: Chemistry Program Office, Office of Naval Research, Arlington, VA 22217	12. REPORT DATE: August 1985
	13. NUMBER OF PAGES
14. MONITORING AGENCY NAME & ADDRESS (if different from Controlling Office)	15. SECURITY CLASS. (of this report): UNCLASSIFIED
	15a. DECLASSIFICATION/DOWNGRADING SCHEDULE

16. DISTRIBUTION STATEMENT (of this Report)

Approved for public release; distribution unlimited

17. DISTRIBUTION STATEMENT (of the abstract entered in Block 20, if different from Report)

18. SUPPLEMENTARY NOTES

To be published in J.Vac.Sci.Technol. B 3 (1985)

19. KEY WORDS (Continue on reverse side if necessary and identify by block number)

Thin metal films - molecular beam epitaxy - GaSb, $AuGa_2$ - phase diagram

20. ABSTRACT (Continue on reverse side if necessary and identify by block number)

A new type of metal/semiconductor junction has been developed. Crystalline thin films of the intermetallic compound $AuGa_2$ have been grown by molecular beam epitaxy on GaSb(001) substrates with the orientation (001)$AuGa_2$ ∥ (001)GaSb, [100]$AuGa_2$ ∥ [100]GaSb. The resulting films have been characterized by Auger electron microscopy, x-ray microprobe analysis, low-energy electron diffraction, electron energy loss spectroscopy, scanning electron microscopy, and Rutherford backscattering. The growth procedure is reported, and is discussed in terms of

/MORE/

DD FORM 1 JAN 73 1473 EDITION OF 1 NOV 65 IS OBSOLETE

S/N 0102-LF-014-6601

UNCLASSIFIED

SECURITY CLASSIFICATION OF THIS PAGE (When Data Entered)

the Au-Ga binary phase diagram. This system is of special interest for contacting technology because the compounds terminate a pseudobinary cut through the Au-Ga-Sb bulk ternary phase diagram, which minimizes the amount of chemical interaction across the metal/semiconductor interface.

ABSTRACTS DISTRIBUTION LIST, 056/625/629

Dr. J. Baldeschwieler
California Inst. of Technology
Division of Chemistry
Pasadena, CA 91125

Dr. S.L. Bernasek
Chemistry Dept.
Princeton University
Princeton, NJ 08544

Dr. J. Butler
Naval Research Laboratory
Code 6115
Washington, DC 20375

Dr. F. Carter
Code 6132
Naval Research Laboratory
Washington, DC 20375

Dr. Richard Colton
Code 6112
Naval Research Laboratory
Washington, DC 20234

Dr. J.E. Demuth
IBM Watson Research Center
PO Box 218
Yorktown Hghts, NY 10598

Dr. D. DiLella
Chemistry Dept.
George Washington Univ.
Washington, DC 20052

Dr. Martin Fleischmann
Chemistry Dept.
Southampton University
Southampton SO9 5NH, England

Dr. T.F. George
Chemistry Dept.
University of Rochester
Rochester, NY 14627

Dr. W. Goddard
Calif. Inst. of Technology
Division of Chemistry
Pasadena, CA 91125

Dr. Robert Gomer
James Franck Institute
University of Chicago
Chicago, IL 60637

Dr. Arnold Green
Quantum Surface Dynamics Br.
Naval Weapons Ctr.- Code 3817
China Lake, CA 93555

Dr. Richard Greene
Code 5230
Naval Research Laboratory
Washington, DC 20375

Dr. M. Grunze
Surface Sci/Technol. Lab.
University of Maine
Orono, ME 04469

Dr. P. Hansma
Physics Dept.
University of California
Santa Barbara, CA 93106

Dr. C.B. Harris
Chemistry Dept.
University of California
Berkeley, CA 94720

Dr. D.E. Harrison
Physics Dept.
Naval Postgraduate School
Monterey, CA 93940

Dr. Irvin Heard
Chemistry & Physics Dept.
Lincoln University
Lincoln Univ., PA 19352

Dr. J.C. Hemminger
Chemistry Dept.
University of California
Irvine, CA 92717

Dr. Roald Hoffmann
Chemistry Dept.
Cornell University
Ithaca, NY 14853

Dr. J.B. Hudson
Materials Division
Rensselaer Polytech. Inst.
Troy, NY 12181

Dr. E.A. Irene
Chemistry Dept.
Univ. of North Carolina
Chapel Hill, NC 27514

Dr. L. Interante
Chemistry Dept.
Rensselaer Polytech. Inst.
Troy, NY 12181

Dr. R.C. Jaeger
Calif. Inst. of Technology
Chemistry & Chemical Engrg.
Pasadena, CA 91125

Dr. J.E. Jensen
Hughes Research Ctr.
3011 Malibu Canyon Rd.
Malibu, CA 90265

Dr. Keith H. Johnson
Metallurgy & Materials Sci.
Mass. Inst. of Technology
Cambridge, MA 01239

Dr. J.T. Keiser
Chemistry Dept.
University of Richmond
Richmond, VA 23173

Dr. L. Kesmodel
Physics Dept.
Indiana University
Bloomington, IN 47403

Dr. K.H. Klaunde
Dept. of Chemistry
Kansas State University
Manhattan KN 66506

Dr. M. Knaur
Hughes Research Laboratory
3011 Malibu Canyon Rd.
Malibu, CA 90265

Dr. W. Kohn
Physics Dept.
University of California
San Diego, CA 92093

Dr. F. Kutzler
Chemistry Dept. Box 5055
Tennessee Tech. University
Cookeville, TN 38501

Dr. M.G. Lagally
Metallurgical & Mining Engrg
University of Wisconsin
Madison, WI 53706

Dr. Ronald Lee
Code R 301
Naval Surface Weapons Ctr.
Silver Spring, MD 20910

Dr. P. Lund
Chemistry Dept.
Howard University
Washington, DC 20059

Dr. Theodore E. Madey
Natl. Bureau of Standards
Surface Chemistry Section
Washington, DC 20234

Dr. R.P. Messmer
Materials Characterization
General Electric Company
Schenectady, NY 22217

Dr. Horia Metiu
Chemistry Dept.
University of California
Santa Barbara, CA 93106

Dr. G.H. Morrison
Chemistry Dept.
Cornell University
Ithaca, NY 14853

Dr. J. Murday
Code 6170
Naval Research Laboratory
Washington, DC 20375

Dr. R.L. Park, Director
Materials Research Ctr.
University of Maryland
College Park, MD 20742

Dr. W.T. Peria
Electrical Engrg. Dept.
University of Minnesota
Minneapolis, MN 55455

Dr. Dan Pierce
Optical Physics Div.
Natl. Bureau of Standards
Washington, DC 20234

Dr. R.M. Plummer
Physics Dept.
Univ. of Pennsylvania
Philadelphia, PA 19104

Dr. D. Ramaker
Chemistry Dept.
George Washington Univ.
Washington, DC 20052

Dr. R. Reeves
Chemistry Dept.
Rensselaer Polytech. Inst.
Troy, NY 12181

Dr. A. Reisman
Microelectronics Center
Research Triangle Park
No. Carolina 27709

Dr. G. Ruhloff
IBM Watson Research Ctr.
PO Box 218
Yorktown Hgts, NY 10598

Dr. Paul Schoen
Code 5570
Naval Research Laboratory
Washington, DC 20375

Dr. S. Siberer
James Franck Institute
University of Chicago
Chicago, IL 60637

Dr. Richard Smardzewski
Code 6130
Naval Research Laboratory
Washington, DC 20375

Dr. G.A. Somorjai
Chemistry Dept.
University of California
Berkeley, CA 94720

Dr. A. Steckl
Electrical & Systems Engrg.
Rensselaer Poly. Institute
Troy, NY 12181

Dr. H. Tachikawa
Chemistry Dept.
Jackson State University
Jackson, MI 39217

Dr. R.P. Van Duyne
Chemistry Dept.
Northwestern University
Evanston, IL 60201

Dr. R.G. Wallis
Physics Dept.
University of California
Irvine, CA 92664

Dr. J.H. Weaver
Chemical Engrg & Materials Sci.
University of Minnesota
Minneapolis, MN 55455

Dr. J.M. White
Chemistry Dept.
University of Texas
Austin, TX 78712

Dr. John W. Wilkins
Atomic & Solid State Physics
Cornell University
Ithaca, NY 14853

Dr. R. Stanley Williams
Chemistry Dept.
University of California
Los Angeles, CA 90024

Dr. N. Winograd
Chemistry Dept.
Pennsylvania State Univ.
University Park, PA 16802

Dr. A. Wold
Chemistry Dept.
Brown University
Providence, RI 02912

Dr. John T. Yates
Chemistry Dept.
University of Pittsburgh
Pittsburgh, PA 15260

Dr. E. Yeager
Chemistry Dept.
Case Western Reserve Univ.
Cleveland, OH 41106

DL/413/83/01
056/413-2

TECHNICAL REPORT DISTRIBUTION LIST, GEN

	No. Copies
Office of Naval Research Attn: Code 413 800 N. Quincy Street Arlington, Virginia 22217	2
Dr. Bernard Douda Naval Weapons Support Center Code 5042 Crane, Indiana 47522	1
Commander, Naval Air Systems Command Attn: Code 310C (H. Rosenwasser) Washington, D.C. 20360	1
Naval Civil Engineering Laboratory Attn: Dr. R. W. Drisko Port Hueneme, California 93401	1
Defense Technical Information Center Building 5, Cameron Station Alexandria, Virginia 22314	12
DTNSRDC Attn: Dr. G. Bosmajian Applied Chemistry Division Annapolis, Maryland 21401	1
Dr. William Tolles Superintendent Chemistry Division, Code 6100 Naval Research Laboratory Washington, D.C. 20375	1
Dr. David Young Code 334 NORDA NSTL, Mississippi 39529	1
Naval Weapons Center Attn: Dr. Ron Atkins Chemistry Division China Lake, California 93555	1
Scientific Advisor Commandant of the Marine Corps Code RD-1 Washington, D.C. 20380	1
U.S. Army Research Office Attn: CRD-AA-IP P.O. Box 12211 Research Triangle Park, NC 27709	1
Mr. John Boyle Materials Branch Naval Ship Engineering Center Philadelphia, Pennsylvania 19112	1
Naval Ocean Systems Center Attn: Dr. S. Yamamoto Marine Sciences Division San Diego, California 91232	1
Ms. Carlena Leufroy Office of Naval Research 1030 East Green Street Pasadena, CA 91106	2

J.Vac.Sci.Technol. B 3 (1985)

016504JBS

Running Title: $AuGa_2$ on GaSb(001): An epitaxial thermodynamically stabilized metal/III–V compound

$AuGa_2$ on GaSb(001): An epitaxial, thermodynamically stabilized metal/III–V compound semiconductor interface

Jeffrey R. Lince and R. Stanley Williams

Department of Chemistry and Biochemistry, University of California, Los Angeles, Los Angeles, California 90024

(Received 31 January 1985; accepted 22 March 1985)

A new type of metal/semiconductor junction has been developed. Crystalline thin films of the intermetallic compound $AuGa_2$ have been grown by molecular beam epitaxy on GaSb(001) substrates with the orientation (001)$AuGa_2$||(001)GaSb, [100]$AuGa_2$||[100]GaSb. The resulting films have been characterized by Auger electron spectroscopy, low energy electron diffraction, electron energy loss spectroscopy, scanning electron microscopy, x-ray microprobe analysis, and Rutherford backscattering. The growth procedure is reported, and is discussed in terms of the Au–Ga binary phase diagram. This system is of special interest for contacting technology because the compounds terminate a pseudobinary cut through the Au–Ga–Sb bulk ternary phase diagram, which minimizes the amount of chemical interaction across the metal/semiconductor interface.

← INDENT

I. INTRODUCTION

The chemistry at interfaces between metals and compound semiconductors is considerably more complex than at interfaces between metals and elemental semiconductors. The extra degree(s) of freedom introduced into the system by using a semiconductor consisting of two (or more) elements in general increases the number of solid phases that may be present at equilibrium.[1] The inability to obtain chemically uniform metal contacts is becoming an important issue in the electronics industry as an increasing number of devices and circuits based on compound semiconductors are developed and as the sizes of these components become smaller. One of the main stumbling blocks in the production of these devices is that electronic properties of the metal/semiconductor interface (e.g., the Schottky barrier height) can be highly dependent on the chemical state at the interface.[2] It is therefore desirable to find metals that are chemically inert with respect to compound semiconductors if stable, reproducible devices that operate at varying temperatures and high power levels are to be fabricated.

In this paper, the molecular beam epitaxial (MBE) growth of a nearly lattice matched and chemically inert intermetallic compound film on a compound semiconductor is reported for the first time. This system, $AuGa_2$ on GaSb, is the structural and chemical analog of $NiSi_2$ on Si.[3] The intermetallic compound $AuGa_2$ has the cubic fluorite crystal structure (as does $NiSi_2$) with a lattice constant of 6.076 Å,[4] which differs from that of GaSb by only 0.5%. Furthermore, the two compounds terminate a pseudobinary cut through the Au–Ga–Sb ternary phase diagram,[5] i.e., they behave like a simple binary eutectic system, with negligible mutual solid solubilities, which means that the bulk solids are thermodynamically stable in contact with each other (no macroscopic chemical reactions) up to the eutectic temperature of the system, when the first liquid forms (i.e., at a temperature less than 764.6 K, the melting point of $AuGa_2$). Thus, at least from a chemical standpoint, such a system should produce an ideal contact to a compound semiconductor device.

II. EXPERIMENTAL

Films have been grown on undoped GaSb substrates with surfaces oriented to within 0.5° of the (001) plane. The substrates were chemomechanically polished with a 2% solution of Br in methanol, and further cleaned in the UHV system (base pressure $\sim 5\times10^{-10}$ Torr) with several cycles of Ar^+ ion bombardment (1.0 keV beam energy) followed by annealing to ~743 K. During MBE growth, beams of Au and Ga from separate sources mounted in a LN_2-cooled deposition system[6] were directed at the sample, which was at 320 K. The growth rate of the $AuGa_2$ film was ~0.2 Å/s, as determined by calibrating the flux from the ovens with a quartz crystal oscillator. Auger electron spectroscopy (AES), low energy electron diffraction (LEED), and electron energy loss spectroscopy (EELS) were performed *in situ*. The samples were then removed and stored in air until they could be analyzed with scanning electron microscopy (SEM), x-ray microprobe (XMP) analysis, and Rutherford backscattering spectroscopy (RBS). In addition, EELS was performed on a $AuGa_2$ single crystal surface that was oriented and polished to within 0.5° of the (001) plane to provide signature spectra to compare with the grown films.

After the UHV *in situ* cleaning was completed, a strong (001)-3×2 LEED pattern with half-order streaking was observed, similar to that reported by Ludeke[7] and Van Bommel and Crombeen.[8] The EELS spectrum for the clean GaSb(001) surface compares fairly well with previously published spectra.[7] Any differences may be accounted for by the difference in beam energy and resolution ($E_0 = 90$ eV and 0.6 eV resolution in Ref. 7 as compared to 300 and 2 eV resolution in the present study).

During the MBE growth of the $AuGa_2$ film, it is important to control the relative flux ratio of Ga and Au ($\alpha = F_{Ga}/F_{Au}$) arriving on the GaSb substrate. To understand why, one may consult the Au–Ga phase diagram.[9] Immediately on the Ga-poor side of the $AuGa_2$ composition at $X_{Ga} = 66.6\%$, $AuGa_2$ coexists with another intermetallic compound (AuGa) below 724 K. On the Ga-rich side of the

$AuGa_2$ composition, there is a eutectic at $X_{Ga} \cong 100\%$ and $T \cong 303$ K. Thus an α of slightly more than 2.0 ($X_{Ga} > 66.6\%$) produces a film of $AuGa_2$ coexisting with a relatively small amount of almost pure liquid Ga, if the substrate temperature is maintained above 303 K. This small amount of liquid Ga would be expected to reside on top of the $AuGa_2$ film because of its surface tension, leaving only $AuGa_2$ and GaSb in contact at the interface. If α falls below two, the film will be heterogeneous and polycrystalline, since there will be two solid phases (AuGa and $AuGa_2$) present at the interface region.

There are also kinetic reasons for controlling α. Simic *et al.*, have shown that in the reaction between Au and Ga thin films at room temperature (RT), there is a significant amount of Au present for >4 days after the deposition for total Ga concentrations (X_{Ga}) between 25–60 at. %.[10] For $X_{Ga} \cong 65\%$ and greater, the Au reacts almost immediately (within 2 min) to form $AuGa_2$. For lower Ga concentrations in a Au–Ga film on GaSb, there could be significant decomposition of the semiconductor, since it has been shown that Au reacts strongly with GaSb.[6,11] Thus, in order to produce a film of single crystalline $AuGa_2$ on a nondecomposed substrate, it is necessary to control the deposition such that a mean α of greater than 2.0 is achieved.

III. RESULTS AND DISCUSSION

After the deposition (with $\alpha = 2.1$) of a nominal 3240 Å $AuGa_2$ film on a GaSb(001) surface, the sample appeared shiny, with only a faint milkiness. LEED showed a good quality (001)-1 × 1 pattern in which the diffraction spots of the film were located with the same relative spacing and orientation as the integral-order spots in the GaSb(001) pattern. The LEED spots of the film were approximately twice the diameter of the spots in the clean GaSb(001) pattern, suggesting that the domain size of the $AuGa_2$ film was about half the domain size of the clean GaSb(001) surface. This pattern persisted after annealing to 573 K, and also after a short ion bombardment and anneal.

AES analysis of the annealed $AuGa_2$ film (see Fig. 1) showed not only the expected Au and Ga, but also the presence of Sb (~1/4 of the Sb detected from the clean GaSb surface). This Sb is depleted by a factor of 8 with a brief (10 min) 0.7-keV-Ar ion bombardment, while the Ga peak-to-peak height is not affected and the Au peak-to-peak height is lowered by <25%. This demonstrates the existence of a thin (<1ML) film of Sb localized near the surface of the $AuGa_2$ film, which may explain why a $AuGa_2$(001)-1 × 1 LEED pattern is seen rather than the expected $c(3 \times 1)$ pattern of the clean $AuGa_2$(001) surface.[12] There might be enough interaction between the $AuGa_2$ surface and the Sb to relax the $AuGa_2$(001)-$c(3 \times 1)$ reconstruction. The sample was briefly ion bombarded and annealed to 483 K several times. Each anneal brought less Sb to the surface than the previous anneal, although increasing the annealing temperature to a maximum of 573 K brought slightly greater amounts of Sb to the surface. In each case, however, the amount of Sb was less than one monolayer. If a Au film of equivalent thickness had been deposited and then heated, roughly 1500 monolayers of Sb would have been produced by the ensuing chemical reaction between the Au and GaSb.[6]

Thus, the quantity of Sb involved compared to the total amount of $AuGa_2$ is very small, and is only detectable because of the surface selectivity of low-energy electron spectroscopies,[13] and the high detection sensitivity of AES for Sb.[14] The $AuGa_2$ film is, therefore, not totally inert with respect to the GaSb substrate, but the extent of chemical interaction is reduced drastically compared to pure Au/GaSb interfaces.

EELS of the annealed 3240-Å $AuGa_2$ film on GaSb(001) is shown in Fig. 2(b). The spectrum is similar to the spectrum of the clean $AuGa_2$(001) surface [see Fig. 2(a)], with any dif-

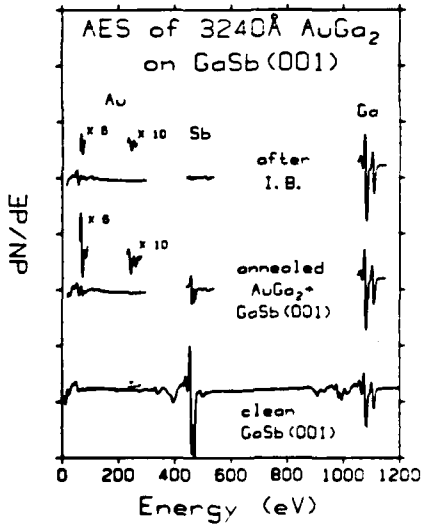

FIG. 1. AES spectra of the clean GaSb(001) surface and the annealed $AuGa_2$ film on GaSb(001), before and after a short ion bombardment. The *M.N.N* Sb doublet is at 454–462 eV, while the main Ga *L.M.M* peak is at 1070 eV. The Au 69 eV peak and the Au 239 eV peak are shown expanded by 6× and 10×, respectively.

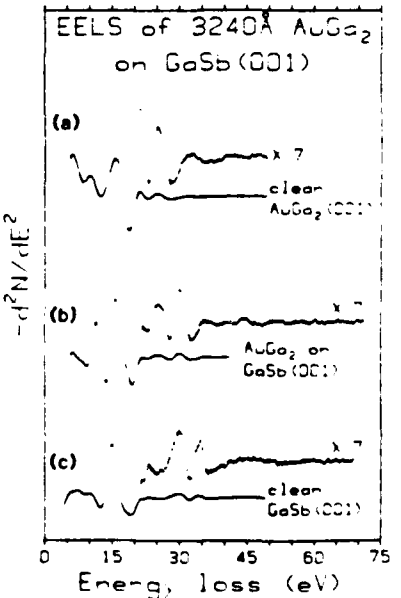

FIG. 2. EELS spectra of (b), the annealed $AuGa_2$ film on GaSb(001), shown with similar spectra for (a) $AuGa_2$(001) and, (c) clean GaSb(001). The electron beam energy was 300 eV for all spectra.

ferences due to the existence of the thin Sb film on the surface. The only major peak in Fig. 2(b) that does not appear in the $AuGa_2$(001) spectra is at $\sim$30 eV. This peak is probably due to a Sb surface-related transition and can be compared to similar transitions of GaSb(001) surfaces, while the Sb bulk-related peak at $\sim$35 eV is conspicuously absent; the peaks at $\sim$21 and $\sim$25 eV in the three spectra in Fig. 2 are due to Ga surface- and Ga bulk-related transitions, respectively, and are similar to transitions in GaAs and GaSb [see Fig. 2(c) and Ref. 7]. Although it is difficult to compare intensities in these EELS spectra because they are taken in second derivative mode, the peak height ratios of the surface and bulk plasmon losses of $AuGa_2$ in Figs. 2(a) and 2(b) (at 11 and 16 eV, respectively) are similar, reinforcing the notion that the film consists predominately of $AuGa_2$.

Figure 3 shows SEM photos of the 3240-Å-$AuGa_2$ film taken at normal electron beam incidence [Fig. 3(a)] and at an angle of 70° from normal [Fig. 3(b)]. Figure 3(a) shows a relatively smooth film with about 30% of the film covered with small depressions (medium-dark areas), while the five larger, darker holes or depressions in the center and right-hand side of the photograph constitute no more than a few percent of the surface. Each of the larger depressions in Fig. 3(a) is adjacent to and in contact with a lighter area of similar size. These light colored regions correspond to the mounds apparent at a 70° electron beam incidence angle, e.g., the large mound visible in the upper right hand corner of Fig. 3(b).

XMP analysis has helped to elucidate the compositions of the depressions and mounds in the film. Analysis of the mound in the upper right in Fig. 3(b) shows a drop in the detected Au and Sb concentrations and a corresponding rise in the Ga concentration as the electron beam incidence angle is decreased (i.e, is moved away from normal). Since this occurs because the incident electrons are sampling less material in the z direction (normal to the surface), one may conclude that the mound consists of some of the excess Ga deposited during film growth.

The relative amounts of Ga and Au in the film are not simply represented by the Ga and Au concentrations that were calculated directly from the XMP data. Some of the detected Ga x-rays originated from the GaSb substrate as well as from the film [X_{Ga}(detected) = X_{Ga}(substrate) + X_{Ga}(film)], since the 20 keV electrons that were used can excite characteristic x-ray emission to a maximum depth of $\sim 1.5\,\mu$m. In order to correct for the substrate Ga, it may be assumed that virtually all of the Sb detected originated from the GaSb substrate, and is roughly equal to the substrate's contribution to the total detected Ga [X_{Ga}(substrate) = X_{Sb}(detected)]. Therefore, the contribution of Ga in the film can be readily calculated by subtracting the detected Sb concentration from the detected Ga concentration [X_{Ga}(film) = X_{Ga}(detected) − X_{Sb}(detected)]. After applying this correction, it was found that the Ga/Au ratio in the film varied from 2.6 to 1.9 ($\pm$ 0.1), depending upon whether or not the area sampled was covered by a mound of excess Ga. The minimum ratio of $\sim$2 further supports the conclusion that the film consists primarily of $AuGa_2$.

XMP analysis of the smaller depressions showed an 80%–90% reduction of the detected Au as compared to the flat portion of the film, with a corresponding increase (20%–30%) in the detected Ga. Although some Sb is detected (from the substrate) in these depressions, it is <60% of the value of the uncovered GaSb substrate. This demonstrates that the small depressions are not areas of bare substrate, but contain a small amount of Ga and of Au, the latter of which is most likely in the form of $AuGa_2$. This is corroborated by the fact

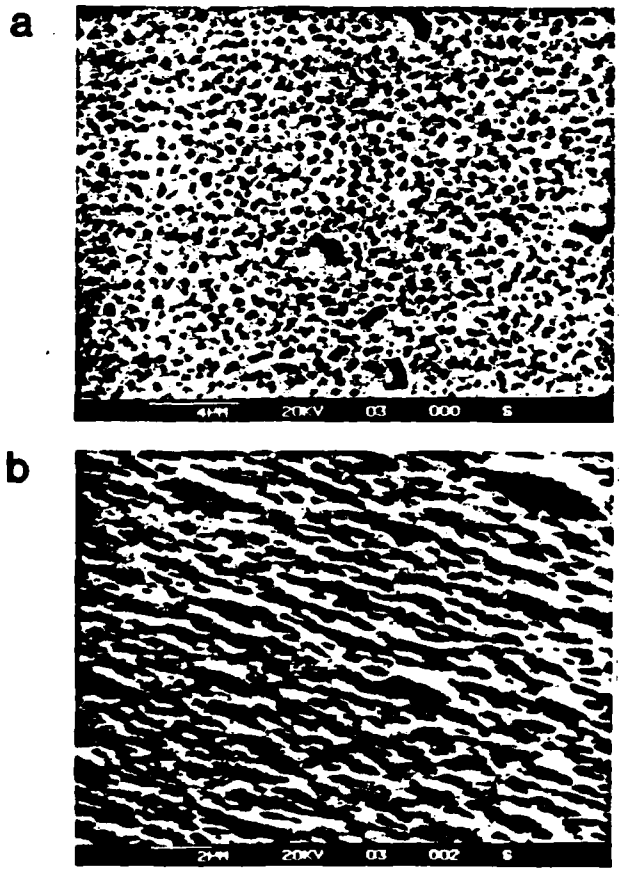

FIG. 3. SEM photographs of the $AuGa_2$ film. Figure 3(a) was produced using normal electron beam incidence and 4500× magnification. Figure 3(b) was taken for an electron beam incidence angle of 70° from the surface normal with 6500× magn. A 20-keV-electron energy was used.

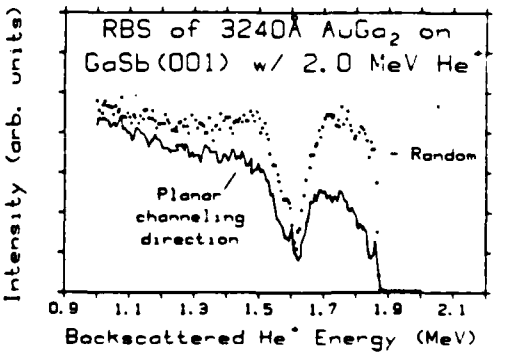

FIG. 4. RBS spectra collected with a 2 MeV incident He^+ beam of the 3240 Å $AuGa_2$ film on GaSb(001). Dotted line: Backscattered He^+ along a random crystallographic direction. Solid line: Backscattering along a planar channeling direction.

that a short ion bombardment reduced the Sb concentration at the surface of the film (as measured by AES) to a value that is ~1/30 of the value of the Sb concentration measured at the surface of clean GaSb(001), whereas the depressions comprise roughly 30% of the surface. However, the five darker, larger areas in Fig. 3(a) could correspond to areas of uncovered substrate, and are perhaps the source of the Sb observed by Auger after ion bombardment.

The observed film morphology also provides a clue to the growth mechanism. The $AuGa_2$ nucleates to form islands,[6] which for the growth conditions reported here grow to a height of approximately 4500 Å before coalescing to form a completely connected network.

RBS was performed on the sample with 2-MeV-He^+ ions incident on both random and planar channeling directions (see Fig. 4). Backscattering in the random direction produced a spectrum with a relatively small difference in slope between the left and right sides of the Au scattering yield, which suggests a fairly small variation in the thickness of the $AuGa_2$ film, and further supports the suggested island growth mechanism. Backscattering in a planar channeling direction revealed Ga and Au surface peaks at 1.6 and 1.85 MeV, respectively. The minmum yield of 0.21 (measured just behind the Au surface peak) demonstrates that a reasonably high degree of crystalline order exists in the film, but the rapid approach of the planar blocking yield to the random yield at energies corresponding to backscattering from the substrate shows that the crystalline order of the film is far from ideal.[16]

There are a number of experiments that still need to be performed to improve the film morphology and crystallinity. Films should be grown using different substrate preparations and temperatures, and varying the deposition parameters, such as the total evaporant flux rate and flux ratio α. These studies should determine whether $AuGa_2$ can form uniform films in order to produce a continuous, abrupt interface. The amount of interfacial strain produced by an epitaxial metal overlayer with 0.5% lattice mismatch would also be examined. Finally, a study of the electrical properties of this metal/semiconductor contact and their variation with temperature should be performed to assess the utility of this system for device applications.

IV. SUMMARY

In conclusion, a metal and a compound semiconductor that terminate a pseudobinary tie line in the bulk phase diagram of the components will form a chemically stabilized interface, since the bulk materials are in thermodynamic equilibrium with one another. Specifically, $AuGa_2$ has been grown epitaxially on GaSb(001) by deposition from separate Au and Ga sources. The resulting films are nearly inert with respect to the semiconductor substrate up to temperatures of at least 573 K, and only a small amount of Sb is released by annealing. In contrast, pure Au films react chemically and consume a large quantity of the GaSb substrate on annealing.[6] In addition, $AuGa_2$ and GaSb are nearly lattice matched, which allows for the growth of epitaxial overlayers. The films grown on ion bombarded and annealed substrates at RT show roughness on the ~1000 Å scale and the crystallinity of the films is only fair. However, further research should enable large improvements in the film quality to be made.

ACKNOWLEDGMENTS

This work was supported by the Office of Naval Research. The authors wish to thank Dr. B. Paine for the RBS results and R. Lysse for the SEM and XMP analyses. One of us (RSW) acknowledges the Camille and Henry Dreyfus Foundation for providing a Teacher–Scholar Grant and the Alfred P. Sloan Foundation for a fellowship.

[1] R. S. Williams, Thin Solid Films (submitted).
[2] L. J. Brillson, Surf. Sci. Rep. 2, 123 (1982).
[3] R. T. Tung, J. M. Poate, J. C. Bean, J. M. Gibson, and D. C. Jacobson, Thin Solid Films 93, 77 (1982).
[4] C. J. Cooke and W. Hume-Rothery, J. Less Common Metals 10, 52 (1966).
[5] C.-T. Tsai and R. S. Williams (to be published).
[6] J. R. Lince and R. S. Williams, Thin Solid Films (submitted).
[7] R. Ludeke, IBM J. Res. Dev. 22, 304 (1978).
[8] A. J. Van Bommel and J. E. Crombeen, Surf. Sci. 93, 383 (1980).
[9] M. Hansen, *Consitution of Binary Alloys* (McGraw-Hill, New York, 1958), p. 205.
[10] V. Simic and Z. Marinkovic, Thin Sol. Films 34, 179 (1976).
[11] P. W. Chye, I. Lindau, P. Pianetta, C. M. Garner, C. Y. Su, and W. E. Spicer, Phys. Rev. B 18, 5545 (1978).
[12] J. G. Nelson, J. R. Lince, W. J. Gignac, and R. S. Williams, J. Vac. Sci. Technol. A 2, 534 (1984).
[13] M. P. Seah and W. A. Dench, Surf. Int. Anal. 1, 2 (1979).
[14] L. E. Davis, N. C. MacDonald, P. W. Palmberg, G. E. Riach, and R. E. Weber, *Handbook of Auger Electron Spectroscopy, 2nd ed.* (Physical Electronics Div., Perkin-Elmer Corp., Eden Prairie, MN, 1978), p. 14.
[15] J. I. Goldstein, in *Practical Scanning Electron Microscopy*, edited by J. I. Goldstein, *et al* (Plenum, New York, 1975), pp. 81–87.
[16] R. S. Williams, L. C. Feldman, and A. Y. Cho, Radiat. Eff. 54, 217 (1981).

LIMIT OF TEXT

OFFICE OF NAVAL RESEARCH

Research Contract N00014-83-K-0612

TECHNICAL REPORT No. 8

COMPARISON OF CHEMICALLY INERT AND REACTIVE METAL/COMPOUND-SEMICONDUCTOR INTERFACES

$AuGa_2$ and Au on GaSb(001)

by

Jeffrey R. Lince and R. Stanley Williams

To Be Published

in

Thin Solid Films

Department of Chemistry and Biochemistry
University of California, Los Angeles, CA 90024

August, 1985

CLASSIFIED

SECURITY CLASSIFICATION OF THIS PAGE (When Data Entered)

REPORT DOCUMENTATION PAGE		READ INSTRUCTIONS BEFORE COMPLETING FORM
1. REPORT NUMBER 8	2. GOVT ACCESSION NO.	3. RECIPIENT'S CATALOG NUMBER
4. TITLE (and Subtitle) COMPARISON OF CHEMICALLY INERT AND REACTIVE METAL/COMPOUND-SEMICONDUCTOR INTERFACES: $AuGa_2$ and Au on GaSb(001).		5. TYPE OF REPORT & PERIOD COVERED Technical Report - Dec 84- Aug 85
		6. PERFORMING ORG. REPORT NUMBER
7. AUTHOR(s) Jeffrey R. Lince and R. Stanley Williams		8. CONTRACT OR GRANT NUMBER(s) N00014-83-K-0612
9. PERFORMING ORGANIZATION NAME AND ADDRESS UCLA Los Angeles, CA 90024		10. PROGRAM ELEMENT, PROJECT, TASK AREA & WORK UNIT NUMBERS
11. CONTROLLING OFFICE NAME AND ADDRESS Chemistry Program Office Office of Naval Research, Arlington VA 22217		12. REPORT DATE August 1985
		13. NUMBER OF PAGES 39
14. MONITORING AGENCY NAME & ADDRESS(if different from Controlling Office)		15. SECURITY CLASS. (of this report) UNCLASSIFIED
		15a. DECLASSIFICATION DOWNGRADING SCHEDULE

16. DISTRIBUTION STATEMENT (of this Report)

Approved for public release; distribution unlimited

17. DISTRIBUTION STATEMENT (of the abstract entered in Block 20, if different from Report)

18. SUPPLEMENTARY NOTES

To be published in Thin Solid Films (1985)

19. KEY WORDS (Continue on reverse side if necessary and identify by block number)

Thin metal films — molecular beam deposition -- Au, $AuGa_2$, GaSb -- ternary phase diagram.

20. ABSTRACT (Continue on reverse side if necessary and identify by block number)

$AuGa_2$/GaSb(001) and Au/GaSb(001) interfaces were prepared by molecular-beam deposition and studied using Auger electron spectroscopy, low-energy electron diffraction, electron energy-loss spectroscopy, scanning electron microscopy, and x-ray microprobe analysis. $AuGa_2$ was chosen as an inert contact because it terminates a pseudobinary tie-line in the Au-Ga-Sb ternary phase diagram. Annealing a 500-Å $AuGa_2$ film (deposited with a small excess of Ga) on GaSb to 747K yielded islands of $AuGa_2$ and Ga, residing on top of a relatively smooth

/MORE/

DD FORM 1 JAN 73 1473 EDITION OF 1 NOV 65 IS OBSOLETE

S N 0102-LF-014-6601

UNCLASSIFIED

SECURITY CLASSIFICATION OF THIS PAGE (When Data Entered)

and flat substrate. In contrast, a 500-Å Au film annealed to 723 K reacted chemically with the substrate, resulting in the formation of islands consisting of Au-Ga compound phase(s) and gross pitting of the GaSb(001) surface. A LEED-AES study of the annealing behavior of a 40-Å Au film on GaSb(001) showed that Au reacts with GaSb even at room temperature. The resultant Au-Ga phase(s) in the film coalesce(s) into islands above ~500 K. The chemical inertness of the $AuGa_2$ and the reactivity of the Au thin films are entirely consistent with the bulk thermodynamic properties of the Au-Ga-Sb system.

Comparison of Chemically Inert and Reactive Metal/Compound-Semiconductor Interfaces: $AuGa_2$ and Au on GaSb(001)

Jeffrey R. Lince* and R. Stanley Williams

Department of Chemistry and Biochemistry
University of California at Los Angeles
Los Angeles, CA 90024

Abstract

$AuGa_2$/GaSb(001) and Au/GaSb(001) interfaces were prepared by molecular beam deposition and studied using Auger electron spectroscopy, Low energy electron diffraction, Electron energy loss spectroscopy, Scanning electron microscopy, and X-ray microprobe analysis. $AuGa_2$ was chosen as an inert contact because it terminates a pseudo-binary tie-line in the Au-Ga-Sb ternary phase diagram. Annealing a 500Å $AuGa_2$ film (deposited with a small excess of Ga) on GaSb to 747K yielded islands of $AuGa_2$ and Ga, residing on top of a relatively smooth and flat substrate. In contrast, a 500Å Au film annealed to 723K reacted chemically with the substrate, resulting in the formation of

---

*Present address: The Aerospace Corporation, Chemistry and Physics Laboratory M2/271, P.O. Box 92957, Los Angeles, CA, 90009 (USA).

islands consisting of Au-Ga compound phase(s) and gross pitting of the GaSb(001) surface. A LEED-AES study of the annealing behavior of a 40Å Au film on GaSb(001) showed that Au reacts with GaSb even at room temperature. The resultant Au-Ga phase(s) in the film coalesce into islands above ~500K. The chemical inertness of the $AuGa_2$ and the reactivity of the Au thin films are entirely consistent with the bulk thermodynamic properties of the Au-Ga-Sb system.

I. INTRODUCTION

The metal / semiconductor contact is the crucial communication link between a semiconductor device and the outside world. In order for an electronic device to operate reliably over long time periods, the interface between the metal and semiconductor should be highly uniform and chemically stable. Chemical reactions that occur after a device has been placed in service will change the operating parameters of the device and most likely result in failure. These concerns are especially valid for high temperature or high power applications, but they have not been especially troublesome for silicon-based technology. Nature has been kind in providing an elemental semiconductor with the utility of Si, since the various types of binary metal/Si systems have relatively few reaction products and simple phase diagrams.

As the electronics industry makes the transition from elemental semiconductor technology to devices made from compound semiconductors (because, for example, of the greater electron mobility of GaAs over Si), it is crucial to find contact materials that will not chemically degrade the metal/semiconductor interface. At the present time, however, the most commonly used contacting material for compound semiconductors is Au. Resultant contacts display great chemical, and therefore electrical instability with increasing temperature. Previous studies have shown that for Au contacts to n-type GaAs, for example, an anneal to only 423K lowered the Schottky barrier height (ϕ_b) by between 6% and 40% and the breakdown voltage (V_B) was reduced by between 10% and 80% (the wide variation in values is perhaps caused by the differences in vacuum and deposition conditions among the

studies).[1,2,3] An anneal to 673K was sufficient to transform the interface into a quasi-ohmic contact.[1,2]

For a better understanding of such changes in the electrical properties of Au contacts to n-type GaAs, examinations of the chemistry at the metal/semiconductor interface have been undertaken.[1-10] An extremely illuminating study was that of Yoshiie, et al.[1], in which the authors used Transmission Electron Microscopy (TEM) and electron diffraction to study the system both parallel and perpendicular to the interface. The study found that annealing the room temperature (RT) deposited film to only 373K was sufficient to produce pyramidal pits in the GaAs substrate. Varying the deposition conditions and subsequently annealing to temperatures up to 603K produced greater pitting and various interfacial compounds, including single crystalline Au, Au_2Ga, and a previously unidentified hexagonal Au-Ga phase. In addition, the Au crystallites formed different crystalline relationships with respect to the substrate depending on the deposition and annealing conditions.

Although the cooling rate was not mentioned in the study by Yoshiie, et al., it is probable that other interfacial reaction products could have been found by varying this parameter. Zeng and Chung have conducted an x-ray diffraction study of the annealing behavior of Au films on n-type GaAs.[10] They found that, by varying the cooling rate after heating the sample to 738K, they were able to observe both Au_7Ga_2 (2.5-40 K/min.) and Au_2Ga (5.2-40 K/min.). In heating from 623K to 729K, the compound AuGa was observed to form. Thus, the reaction products observed are dependent on kinetic, as well as on thermodynamic considerations.

Guha, et al.,[3] have compared the Schottky barrier heights ϕ_b for two types of samples: (1) Au/n-GaAs Schottky diodes, and (2) Schottky diodes made by flash depositing a Au-Ga alloy (85%Au-15%Ga) onto an n-GaAs substrate. This study found that the ϕ_b of the Au/GaAs diodes dropped by .35 eV after annealing to 673K, while the ϕ_b of the (Au-Ga)/GaAs diodes dropped by only .04 eV under the same annealing conditions. Thus, the addition of Ga to the Au metallization appears to stabilize the electrical properties of the contact. This stabilization is most likely due to a decreased chemical interaction between the metal and the GaAs.

Sebestyen, et al., have studied the As loss (in the form of As_2) from various metal/GaAs contacts as the temperature is ramped.[11] They found that sequentially deposited Au and Ga layers (Au/Ga/Au-GaAs: the Ga concentration in the deposited layers was ~39%) produced contacts that evolved an amount of As_2 that was a factor of ~4 less than with Au/GaAs contacts. The As_2 that was evolved from the layered structure was, however, greater than for other contacts (i.e. Ag, CrAu, Pt, and Al).

Although the studies by Guha[3] and Sebestyen[11] show important, preliminary results for Au-Ga co-evaporation on GaAs, neither has taken the effect of the Ga:Au ratio into account. In both cases, there was less than 66.6 At% Ga in the deposited films. There is reason to believe that the contacts would have shown even less decomposition if they had used a Ga:Au ratio ≥2. This is demonstrated in a study by Simic, et al.,[12] in which Au and Ga thin films were sequentially deposited on a glass substrate and analyzed visually and with x-ray

diffraction for evidence of chemical reaction at RT. It was found that for Au-Ga films with between 25-60 At% Ga, there was a large amount of Au present for at least 4 days at RT. For films with ~65% Ga and greater, the Au reacted almost immediately (within a few minutes) to form $AuGa_2$. Therefore, even though some Ga was co-deposited with Au in both the Guha and Sebestyen studies, not enough Ga was deposited to react to completion with the Au, and the excess Au reacted with the GaAs substrate.

There have been fewer studies of the Au/GaSb interface, but the ones that exist also reveal interfacial chemical reactions.[13,14] Chye, et al., observed with Soft X-ray Photoelectron Spectroscopy (SXPES) that Sb appeared on the surface of Au films deposited on GaSb(110) substrates at RT, indicating some type of chemical interaction between Au and GaSb. Also, Ar^+ ion depth profiling methods were used in combination with AES, which showed that significant amounts of Ga were present along with the Au in the film. The depth profiles also showed that Sb was present in the top few layers of the Au film, but not in the bulk of the film. The presence of this Sb was interpreted by Chye, et al. in terms of $AuSb_2$ formation at the surface.[13]

Koshizaki, et al., have used Angle-Resolved X-ray Photoelectron Spectroscopy (ARXPS) to study the Au/GaSb(110) interface. They found evidence of chemical reaction of the Au with the substrate after annealing an 85Å Au film to 673K. This was shown by the chemical shift of the Au-$4f_{7/2}$ peak, and the disappearance of Au-5d splitting after annealing. They also studied the effect of varying the surface-detector angle on the intensity of the photoelectron peaks. Variation

in the angular distribution curves (ADC's) can be the result of photoelectron diffraction, and are therefore indicative of crystalline order. After annealing the sample to 813K for 30 min., they found that the ADC's for the Au-4f and Ga-3d peaks were similar. This was interpreted in terms of Au atoms incorporating into the GaSb lattice and preferentially substituting for Ga atoms.[14]

A study of the epitaxial growth of $AuGa_2$ on GaSb(001) has been undertaken recently.[15] LEED and Rutherford Backscattering (RBS) studies showed that the $AuGa_2$ film was crystalline, and that the lattice of the film was in registry with the GaSb (i.e. $AuGa_2(001)\|GaSb(001)$ with $AuGa_2[100]\|GaSb[100]$). The lattice misfit in this system is only 0.5% (lattice constant ($AuGa_2$) =6.076Å)[16]. The stoichiometry of the film was examined with X-ray Microprobe Analysis (XMPA), which showed that the film consisted primarily of $AuGa_2$ with some mounds of excess Ga. With a combination of AES and Ar^+ ion bombardment, it was determined that the surface of the $AuGa_2$ film was covered with <1 monolayer (ML) Sb, which is liberated from the GaSb substrate during the growth process. The existence of this relatively small amount of Sb suggests a correspondingly small chemical interaction at the interface. This system is essentially the structural analog of $NiSi_2$ on Si,[17] since $AuGa_2$ has the cubic fluorite structure (same as $NiSi_2$) and the diamond (Si) and zinc-blende (GaSb) structures are closely related.

The choice of the intermetallic compound $AuGa_2$ as a chemically stabilized contact to GaSb was made because $AuGa_2$ and GaSb terminate a pseudo-binary tie-line in the Au-Ga-Sb phase diagram,[18] i.e. the bulk compounds are thermodynamically stable with respect to one another.

Thus, one would expect an abrupt, non-degraded interface between the two bulk phases. The solidus portion of the Au-Ga-As phase diagram is very similar to that of Au-Ga-Sb (i.e. GaAs also terminates a pseudo-binary tie-line with $AuGa_2$),[19] so the use of $AuGa_2$ as a chemically inert metal contact is also valid for GaAs.

This paper will demonstrate the different behavior of chemically inert and reactive metal/compound-semiconductor interfaces by contrasting the chemical and structural properties of $AuGa_2$ and Au deposited on GaSb(001). These systems were characterized with Auger Electron Spectroscopy (AES), Low Energy Electron Diffraction (LEED), Electron Energy Loss Spectroscopy (EELS), Scanning Electron Microscopy (SEM), and X-ray Microprobe Analysis (XMPA). The remainder of this paper will be organized as follows. Section II describes the experimental details. The experimental results are presented and discussed in section III and are divided into three parts. Part A discusses the substrate characterization. Part B presents the results for $AuGa_2$ films on GaSb(001), while part C presents the results for Au on GaSb(001). Finally, the most important observations are summarized in section IV.

II. EXPERIMENTAL PROCEDURE

All GaSb(001) samples used in this study were undoped. The crystalline orientation of the samples was determined with Laue x-ray diffractometry. The substrates were cut and polished such that the surfaces were within .5° of the (001) plane. After mechanical polishing with 5, .3, and .05 μm alumina in H_2O, the samples were degreased in distilled acetone and methanol. They were then chemo-mechanically polished for about 10 min. using a 2% Br in methanol solution, rinsed in methanol, and air-dried before being mounted in a Varian Ultra-high Vacuum (UHV) analysis chamber equipped for in situ Molecular Beam Epitaxy (MBE). The base pressure was ~5×10^{-10} torr during the measurements. The sample was heated by placing it in contact with a thin piece of resistively heated Ta foil. The sample temperature was measured using a Pt/Pt-10% Rh thermocouple (TC) that was spot-welded to the Ta foil and placed in contact with the backside of the GaSb(001) sample.

The samples were cleaned further in vacuo with several alternating cycles of Argon ion bombardment at 1 keV and annealing to ~743K for 10 min. The degree of sample order was observed by LEED obtained with Varian model 981-0127 optics. AES and EELS spectra were collected with a PHI model 11-500 single-pass cylindrical mirror analyzer (CMA). The resolution of the CMA was set at 3 eV for AES and 2 eV for EELS. For both techniques, the output from the lock-in amplifier was passed into an analog-to-digital converter interfaced to an LSI 11/23 microcomputer. The numerical data were stored on floppy disks and later analyzed on a VAX 11/780 computer. AES showed either no

detectable contaminants or a total carbon and oxygen contamination of <.02 ML.

The MBE system consisted of an 8 in. Conflat flange that supported three thermally separated compartments, each of which contained an evaporator. All three sources sat inside a LN_2-cooled shroud to avoid excessive outgassing during the deposition. Each source had independent feedthroughs for shuttering the source, controlling the source temperature, and reading the temperature. The Ga source was a Knudsen effusion cell that was constructed of a Boron nitride (BN) crucible wrapped in a tightly wound coil of .010 in. diameter, high purity T. wire. This section was then covered with a BN sleeve and wrapped with Mo foil for radiative heat shielding. The temperature of the cell was measured by a W/W-5%Re TC placed through a 1/16 in. hole in the sleeve in contact with the rear of the crucible. The Au source consisted of a .010 in. diameter, high purity W filament wound into a 1/8 in. diameter basket.

The binary phase diagram of the metals that form the intermetallic compound $AuGa_2$ must be taken into account when designing the MBE-grown contact. The Au-Ga phase diagram[20] shows that for a Ga:Au ratio a little lower than 2 (i.e. $50\% < X_{Ga} < 66.6\%$), solid $AuGa_2$ coexists with solid AuGa at temperatures $\leq$724K. The existence of two solid phases in the film would preclude the growth of a homogeneous, single-crystalline metal film on the semiconductor. This would result in a contact with electrical properties that would vary widely between microscopic regions of the surface. Integrated circuits with small features would perform unpredictably, especially if the polycrystalline grain size in

the film was comparable to the feature size. For a Ga:Au ratio greater than 2 (i.e. $66.6\% < X_{Ga} < 100\%$), solid $AuGa_2$ coexists with liquid Ga in the temperature range 303-765K. MBE growth of a complete film in this range of concentrations and substrate temperatures should produce a homogeneous contact, since the liquid Ga should 'float' away from the solid-solid interface to the surface of the $AuGa_2$ film in the process of forming droplets to minimize the free energy of the liquid Ga surface.

The $AuGa_2$ was deposited by exposing the sample (sample temp.=320K) to both sources simultaneously and periodically closing one shutter for a length of time that would compensate for flux rates that deviated slightly from the desired stoichiometry. The flux ratio for the $AuGa_2$ deposition, $\alpha = F_{Ga}/F_{Au}$, was held at an average of ~2.2 to ensure that the composition of the deposited film was toward the Ga side of $AuGa_2$ on the Au-Ga phase diagram. For the Au depositions, the substrate temperature was measured to be 310K. Au and $AuGa_2$ deposition rates were approximately 0.1 and 0.2 Å/sec., respectively.

The background pressure rose to 1×10^{-8} torr during initial film growth, and fell back to the mid 10^{-9} torr range as the deposition progressed. Deposition rates and film thicknesses were determined with an Inficon model XTM quartz crystal micro-balance. In order to correct for geometric effects during the calibration procedure, the XTM was mounted on a linear drive system that allowed the quartz crystal to be placed in the same position as the sample during the deposition. The deposition geometry was the same for all the studies reported here. The resultant films showed the same low levels of carbon and oxygen

contamination as the clean substrate. After the in situ experiments were completed, the samples were stored in air until they could be studied with SEM and XMPA.

III. RESULTS AND DISCUSSION

A. Substrate Characterization

After the UHV in situ cleaning was completed, a strong (001)-3×2 LEED pattern with half-order streaking was observed that exhibited (001)-c(6×2) spots at some energies. The 3×2-like and c(6×2) patterns correspond to the so-called cation- and anion-stabilized structures discussed by Ludeke.[21] It was reported that the c(6×2) pattern appeared during MBE growth of GaSb(001) under Sb-rich conditions, while the 3×2-like pattern was generated by heating the MBE-grown substrate to >773K. In the present study, the clean GaSb(001) surface probably consisted of both cation- and anion-stabilized terraces, which produced the observed LEED pattern. Such a structure is feasible because the surface was prepared by ion bombardment and annealing to below 773K rather than by MBE.

B. $AuGa_2$ on GaSb(001)

The co-deposition of Au and Ga (a=2.2) produced the equivalent of 496Å of $AuGa_2$ on the clean GaSb(001) surface, which was subsequently annealed to 747K for 20 min. After the in situ LEED, AES, and EELS were performed, the sample was removed into air and analyzed using SEM and XMPA.

SEM of the annealed 496Å $AuGa_2$ film with the electron beam normal to the surface is shown in Fig. 1a, and shows a relatively flat, undisturbed substrate with ~25% of the surface covered by islands with no apparent macroscopic alignment with respect to the surface. The photograph shows that the anneal melted the $AuGa_2$, which has a bulk

melting point of 763K, and that the liquid $AuGa_2$ apparently does not wet the GaSb substrate. The photo in Fig. 1b was taken with the same conditions as in Fig. 1a, except at an electron beam incidence angle of 52° to normal, and reveals a slight ripple in the surface of the semiconductor substrate. Some of the islands in the photographs appear to consist of two distinct phases. This is not surprising, since the deposition was performed with an excess of Ga.

XMPA was performed during the SEM analysis. In order to successfully interpret the XMPA data, the relative amounts of Ga and Au in the islands must not be assumed to be simply represented by the Ga and Au concentrations that were calculated directly from the XMPA data. Some of the detected Ga x-rays originated from the GaSb substrate as well as from the islands ($X_{Ga}(detected)=X_{Ga}(substrate)+X_{Ga}(island)$), since the 20 keV electrons that were used can excite characteristic x-ray emission to a maximum depth of ~ 1.5 μ.[22] In order to correct for the substrate Ga, it may be assumed that virtually all of the Sb detected originated from the GaSb substrate, and is roughly equal to the substrate's contribution to the total detected Ga ($X_{Ga}(substrate)=X_{Sb}(detected)$). Therefore, the contribution of Ga in the islands can be readily calculated by subtracting the detected Sb concentration from the detected Ga concentration ($X_{Ga}(island)=X_{Ga}(detected)-X_{Sb}(detected)$). After applying this correction, Ga/Au ratios were found that ranged from 2.0 ($AuGa_2$ island) and 4.8 (two phase island) to 19 (Ga island). The areas between the islands showed no detectable Au.

Immediately after the deposition of 496Å $AuGa_2$, a fair to good

quality (001)-1×1 LEED pattern was seen, which showed that the film had grown epitaxially. The spot size was 2-3 times the diameter of the integral-order spots of the clean GaSb(001) pattern, indicating that the $AuGa_2$ domain size was 1/2 to 1/3 the domain size of the clean GaSb(001) surface. This smaller domain size could be due to dislocations and other defects in the $AuGa_2$ overlayer. These dislocations could result from the small lattice mismatch between $AuGa_2$ and GaSb (~0.5%). The (001)-1×1 pattern was also seen in the as-deposited 3240Å film[15] and in a 50Å $AuGa_2$ film in this study. After a 20 min. anneal to 747K, the LEED pattern was a strong (001)-1×1 pattern, with third order spots apparent at some energies that resembled the LEED pattern of the clean GaSb(001) surface.

Fig. 2 shows the Auger spectra of the as-deposited and annealed $AuGa_2$ films in comparison to the clean GaSb(001) surface. The spectra from the as-deposited 496Å $AuGa_2$ film in Fig. 2 are very similar to spectra taken from the 3240Å film,[15] i.e. the peak-to-peak heights of the respective elements are the same to within 10% between the two spectra. This suggests that prior to annealing, the $AuGa_2$ film was fairly uniform over the substrate surface. As mentioned above, the Sb peak represents a film (<1 ML) of Sb localized at the surface of the $AuGa_2$ film. The process by which the Sb is liberated from the substrate is not known, but may be due to the heat of condensation of the evaporants, or the heat of formation of $AuGa_2$ on the GaSb surface. The amount of Sb involved, however, is much less than the total $AuGa_2$ present in the film, so its presence suggests a correspondingly small chemical interaction at the interface. This Sb is only detectable

because of the surface selectivity of electron spectroscopies,[23] and the high Auger excitation probability for Sb.[24] With the anneal, the Au peak intensity drops sharply, the Ga peak drops to approximately the value for the clean GaSb(001) surface, while the Sb peak height increases to 73% of the value for the clean GaSb(001) surface. This observation is consistent with the SEM images.

Fig. 3 shows the progression in the EELS spectra as the GaSb(001) surface is covered with varying amounts of $AuGa_2$ and followed by annealing to >573K. The EELS spectrum for the clean GaSb(001) surface in Fig. 3c agrees fairly well with previously published spectra.[21] Any differences can be accounted for by the differences in the primary electron beam energy and resolution (E_0=90 eV and 0.6 eV resolution as compared to E_0=300 eV and 2 eV resolution in the present study). Assignments for the labeled peaks in Fig. 3 are listed in Table I. As might be expected for the spectrum of the annealed 496Å $AuGa_2$ film, the Ga peaks (peaks J and K) are larger (due to the deposition of $AuGa_2$) and broader (due to the difference in chemical shifts between the Ga(3d)-CB peaks for GaSb and $AuGa_2$) than peaks Q and R in Fig. 3c. The excitation represented by peaks M and T arises from an Sb bulk excitation, and predictably is absent in Fig. 3a since the GaSb substrate is completely covered. The Sb surface-related feature (peak F), however, is apparent in Fig. 3a, because of the existence of the partial Sb monolayer mentioned above.

The one EELS feature that does not seem to change much as the film covers more of the surface is the intense, broad peak at ~15 eV (peaks C,I,P). This can be attributed to the bulk plasmon losses of $AuGa_2$

and/or GaSb, since they are calculated to be only ~0.8 eV apart. They will not be resolvable, as plasmon losses are quite broad, and the instrumental resolution is 2 eV in this study. The surface plasmon loss peak at ~11 eV (peaks B,H,O) grows larger as more of the surface is covered by $AuGa_2$. This progression can be seen because peak O, the surface plasmon loss in GaSb, is very small (see Fig. 3c and Ref. 21).

To summarize this section, LEED and AES showed that the as-deposited $AuGa_2$ film grows epitaxially on, and completely covers the GaSb(001) substrate for thicknesses greater than 40Å. SEM shows that annealing of films that are less than ~3000Å thick causes coalescence of the $AuGa_2$ into islands. In particular, a 496Å $AuGa_2$ film, when annealed to 747K, formed islands that covered about 25% of the GaSb surface, which demonstrated minimal decomposition as a result of chemical interaction at the interface. The annealed surface displayed a strong LEED pattern characteristic of clean GaSb(001), which is a good indication that, before annealing, the GaSb/$AuGa_2$ interface was nearly abrupt on an atomic scale. If this were not true, the exposed GaSb surface would be considerably more disrupted. This behavior is very similar to the annealing behavior of Ag on Ge(001),[25] a metal/semiconductor system for which the two components have negligible solid solubilities in one another and do not form any compounds.

C. Au on GaSb(001)

As a preliminary experiment, 4Å of Au were deposited on a clean GaSb(001) surface. No LEED pattern was seen, but after heating the sample to ~650K for 3 min., there was no Au detected with AES and a

sharp GaSb(001)-3×2,c(6×2) LEED pattern was seen, showing a return to the reconstruction of the clean GaSb(001) surface.

506Å of Au were deposited on a clean GaSb(001) surface, which was subsequently annealed to 723K for 15 min. After the in situ LEED, AES, and EELS were performed, the sample was removed into air and analyzed using SEM and XMPA.

The SEM photos of the annealed 506Å Au film in Fig. 4 are in striking contrast to the photos of the annealed 496Å $AuGa_2$ film in Fig. 1. The edges of the rectangular islands in Fig. 4 are oriented with respect to one another and, since each island is not in physical contact with the other islands, they must be aligned along bulk crystalline axes of the substrate. Also, some of the rectangular islands have receded, revealing etched depressions in the GaSb surface in the shape of the islands. This SEM photo is remarkably similar to the bright-field Transmission Electron Microscope (TEM) photograph of an annealed 300Å Au film on GaAs(001) studied by Yoshiie, et al.[1] They also reported TEM cross-sections of the film/surface interface. Their photographs show that the rectangular islands on the surface consist of Au and Au-Ga phases that occupy pyramidal pits, which may be as deep as several thousand Ångstroms, in the GaAs substrate and are bounded by GaAs(111) planes. Thus, the annealing behavior of Au is seen to be very similar on both GaAs and GaSb.

XMPA of the large, rectangular islands show their corrected Ga/Au ratio to be 1.06±.04, with less than 0.5% of Sb detected. This observation suggests that the intermetallic compound AuGa has formed islands that are roughly 1 μm deep. The substrate areas between the

islands are Au free, while analysis of the smaller rectangular pits shows about half the detected Au as in the larger islands.

Immediately after the deposition of 506Å Au, the Auger spectrum of the as-deposited film (see Fig. 5) shows its surface to be free of Ga (within the limits of Auger detectability: ~.5% of a ML) suggesting that prior to annealing, the film is continuous. It is not ordered, however, as unannealed Au films on GaSb with thicknesses of 4Å, 40Å and 500Å showed no discernable LEED pattern. The Auger spectra of the as-deposited Au film yield information consistent with the SXPES spectra in Ref. 13, which finds that, after the deposition, the Ga-3d peak disappears while a noticeable Sb-4d peak is observed.

The surface concentration of Sb on the as-deposited Au film (Fig. 5b) demonstrates that some chemical interaction between Au and GaSb occurs at RT, the freed Sb diffusing to the surface. After the anneal, the Auger spectra in Fig. 5a were taken. They show a Ga peak height that is essentially the same as for the clean surface. The Sb peak is somewhat higher (~60%) than the corresponding Sb peak in the spectrum of the annealed 500 Å $AuGa_2$ film (Fig. 2a), and ~5% higher than the peak for the clean GaSb(001) surface (Fig. 5c), suggesting the presence of excess Sb on the substrate surface. Also, the Au peaks in Fig. 5a drop in intensity by a factor of ~3 from the as-deposited case. This suggests that any Au-Ga phases that are forming are agglomerating into islands and/or diffusing into the GaSb bulk.

The EELS spectra of the as-deposited 506 Å Au film is shown in Fig. 6b. All of the peaks (except for those labeled U and V) are at the same positions as electron energy losses seen in previous studies

of polycrystalline Au,[26,27] although the intensities of the peaks in these studies vary widely with different substrate preparation, electron beam energy, and experimental environment. Peak V probably represents the Sb(4d)→surface state excitation, as in Fig. 3. The origin of peak U is uncertain, but could result from the interaction of the surface Sb with the Au film, e.g. $AuSb_2$ formation. In general, the spectra in Fig. 6b are not similar to any of the other spectra discussed so far, and exhibit a very small bulk plasmon loss that is typical of noble metals. EELS of the annealed Au film (see top of Fig. 6) essentially shows regeneration of the GaSb(001) surface with the low energy Au peaks slightly visible.

A 40Å Au film was then deposited on a new, similarly prepared GaSb(001) sample, which was progressively heated to higher and higher annealing temperatures. Fig. 7 shows the dependence of the Ga/Au Auger peak-to-peak height ratio, the Au Auger peak-to-peak height, and the LEED pattern on the annealing temperature (data were taken at RT). The Au surface concentration dropped off almost exponentially to ~5% of the as-deposited value. This behavior alone cannot distinguish between island formation or diffusion into the bulk. The observed Ga/Sb ratio initially drops between 373K and 493K, and is caused by a rise in the intensity of the Sb Auger peak. The appearance of the 5×2-like LEED pattern in addition to 3×2-like pattern also suggests the existence of excess Sb at the surface, since Ref. 21 states that a GaSb(001)-5×2 LEED pattern can be generated by exposing the sample to an Sb molecular beam below 623K. As the annealing temperature is increased above 493K, the Ga/Sb ratio begins rising again and is caused by a steady increase

in the detected Ga, and a slow decrease in the detected Sb. Above 623K the 5×2 pattern disappears and is replaced by the characteristic pattern of the clean ion-bombarded and annealed GaSb(001) surface.

Our data, and previous results for the Au/GaSb system can be interpreted in terms of assumptions for which reactions are occurring, and estimates of their Gibbs free energies (ΔG_{rxn}) using some simple thermodynamic arguments. This discussion has been outlined for the Au/GaAs system in Ref. 28. Some possible reactions occurring in the Au/GaSb system are listed in Table II. The temperature dependence of the Gibbs free energies of formation of the reactants and products can be estimated[29,30] from the equation:

$$\Delta G_F^T = \Delta H_F^T - T\Delta S_F^T$$

$$= \Delta H_F^{298} + \Delta C_p(T-298)$$

$$- T(\Delta S_F^{298} + \Delta C_p(\ln T - \ln 298))$$

This equation was evaluated for GaSb from its enthalpy of formation (ΔH_F), entropy of formation (ΔS_F), and heat capacity (C_p) values.[31] ΔG_F^T equations for AuGa and $AuGa_2$ were estimated from their ΔH_F values[32] and the Debye theory.[33,34] $\Delta G_{vap}(Sb(s) \rightarrow \frac{1}{4}Sb_4(g))$ was determined from the equilibrium vapor pressure of Sb_4 over solid Sb[35] and assuming that in a UHV chamber, the vapor pressure of Sb_4 was maintained at $\sim 10^{-9}$ torr over the sample during the annealing.

All ΔG_{rxn} vs. T curves for the reactions in Table II have a

negative slope. The reactions become favorable when the temperature exceeds the point at which $\Delta G_{rxn}=0$. Unfortunately, the possibility that other reactions could occur cannot be investigated theoretically in the present study since thermochemical data are not presently available for the more Au-rich phases than AuGa that might be forming. Another limitation is that kinetics might play a role in the interfacial reaction in that it cannot necessarily be assumed that the predicted reaction has proceeded to completion in our study.

The analysis summarized in Table II is consistent with the data in the present study. The detected Ga:Au ratio of ~1 in the islands formed by annealing 506Å Au on GaSb(001) to 723K is not surprising, since one would expect AuGa formation at room temperature. In fact, other studies have shown that the AuGa-GaSb section through the ternary phase diagram is pseudobinary.[18] Also, Fig. 7 may be examined in light of this discussion. The initial drop in the Ga/Sb ratio, caused by a rise in the surface concentration of Sb, may be interpreted in terms of reaction between Au and GaSb with liberation of the resultant Sb through the surface region. Some of this excess Sb adsorbs on the surface, resulting in the decrease in the Ga/Sb ratio. The rise in the Ga/Sb ratio above 493K, and the appearance of a LEED pattern, is a result of continued Au-Ga phase formation, followed by coalescing of these phases into islands, which exposes portions of the Sb-rich GaSb substrate. Finally, the decrease in detected Sb above 650K, along with the disappearance of the 5×2 LEED pattern, is due to desorption of Sb from the Sb-rich GaSb(001) surface.

Our observation of island formation differs from the conclusions

of Koshizaki, et al.,[14] i.e. that the Au atoms were incorporated into the GaSb lattice with annealing. Their data, however, are consistent with the present observations. After their sample was annealed to 673K, the Ga-3d and Sb-4d ADC's were representative of the clean GaSb(110) surface, while the Au-4f ADC showed little structure. This indicates AuGa formation, since its rhombohedral structure discourages lattice match with the cubic GaSb substrate. After annealing to 813K, they found similarities in the Au-4f and Ga-3d ADC's. These similarities might be accounted for by $AuGa_2$ formation, since $AuGa_2$ and GaSb have the same lattice constant. Moreover, it has been shown that $AuGa_2$ will align itself crystallographically with the GaSb lattice at the interface,[15] and Au and Ga occupy similar sites in the $AuGa_2$ lattice. The analysis summarized in Table II is consistent with our conclusion of $AuGa_2$ formation in their study, since it is demonstrated that $AuGa_2$ formation can become favorable for T>560K for a background Sb_4 pressure of 10^{-9} torr. The temperature at which $AuGa_2$ would be formed will be higher under higher Sb_4 pressures.

IV. SUMMARY

The chemistry of thin films of $AuGa_2$ and Au on GaSb(001) substrates has been studied using EELS, AES, LEED, SEM, and XMPA. It has been shown that a $AuGa_2$ film can be grown epitaxially on GaSb(001), forming a nearly abrupt interface. The resultant film remains chemically stable from RT to 743K, although a small amount of Sb is released upon deposition and the film itself melts on annealing to higher temperatures. This stability is a result of the fact that $AuGa_2$ and GaSb terminate a pseudo-binary tie-line in the Au-Ga-Sb ternary phase diagram. The study of the interaction of thin films of Au with GaSb(001) surfaces showed that on annealing to >723K, there is formation of the intermetallic compound AuGa at the interface, resulting in etch pits in the GaSb surface. This observation is consistent with bulk thermodynamic arguments, which show that AuGa formation can occur at room temperature. A LEED-AES annealing study of very thin films has shown that a chemical reaction, and the resultant release of Sb, occurs at 300K, while coalescence of the reacted Au-Ga phase(s) occurs for T>500K. The presence of the excess Sb results in an Sb-rich surface reconstruction for T≥500K. The Sb is desorbed upon annealing for T≥623K, resulting in the regeneration of the annealed, 3×2-like GaSb(001) surface, with areas covered by AuGa.

ACKNOWLEDGMENTS

This work was supported by the Office of Naval Research. The authors wish to thank B. Mueller at the UCLA Molecular Biology Institute for the SEM photographs and R. Lysse at the UCLA Department of Materials Sciences and Engineering for the XMP analyses. One of us (RSW) acknowledges the Camille and Henry Dreyfus Foundation for providing a Teacher-Scholar Grant and the Alfred P. Sloan Foundation for a fellowship.

Table I. Assignments for EELS Peaks in Figs. 3 and 6

labels in Figs. 3,6				Energy (eV)	Assignment
3a	3b	3c	6		
A	G			6-8	Au(5d)→CB
	G	N		6-8	GaSb VB→CB
B	H			11-12	surface plasmon: $AuGa_2$
	H	O		11-12	surface plasmon: GaSb
C	I			15-16	bulk plasmon: $AuGa_2$
	I	P		15-16	bulk plasmon: GaSb
D	J	Q		22	Ga(3d)→ surface state
E	K	R		24-25	Ga(3d)→CB
F	L	S	V	30	Sb(4d)→ surface state
	M	T		35	Sb(4d)→CB
			U	18	$AuSb_2$ transition (?)
			W	33	Au transition

Table II. Possible reactions occurring in the Au/GaSb system

Reaction	$T(\Delta G_{rxn}=0)$ (±30K)
$Au(s)+GaSb(s) \rightarrow AuGa(s)+Sb(s)$	<273K
$AuGa(s)+GaSb(s) \rightarrow AuGa_2(s)+\frac{1}{2}Sb_4(g)^*$	~560K
$GaSb(s) \rightarrow Ga(l)+\frac{1}{4}Sb_4(g)^*$	~620K

---

* at 10^{-9} torr

REFERENCES

1. T. Yoshiie, C.L. Bauer, and A.G. Milnes, Th. Sol. Films 111(1984) 149.
2. B.J. Baliga, R. Ehle, A. Sears, P. Campbell, W. Garwacki, and W. Katz, IEEE Elec. Dev. Lett. 3(1982) 177.
3. S. Guha, B.M. Arora, and V.P. Salvi, Sol. St. Elec. 20(1977) 431.
4. L.J. Brillson, Th. Sol. Films 89(1982) 461.
5. D.C. Miller, J. Electrochem. Soc. 127(1980) 467.
6. A.K. Sinha and J.M. Poate, in Thin Films-Interdiffusion and Reactions, ed. by J.M. Poate, et al. (Wiley-Interscience, New York, 1978) Chap. 11.
7. T. Narusawa, N. Watanabe, K.L.I. Kobayashi, and H. Nakashima, J. Vac. Sci. Technol. A 2(1984) 538.
8. W.G. Petro, I.A. Babalola, T. Kendelewicz, I. Lindau, and W.E. Spicer, J. Vac. Sci. Technol. A 1(1983) 1181.
9. E. Kinsbron, P.K. Gallagher and A.T. English, Sol. St. Elec. 22(1979) 517.
10. Xian-Fu Zeng and D.D.L. Chung, Sol. St. Elec. 27(1984) 339.
11. T. Sebestyen, I. Mojzes, and D. Szigethy, Electr. Lett. 16(1980) 504.
12. V. Simic and Z. Marinkovic, Th. Sol. Films 34(1976) 179.
13. P.W. Chye, I. Lindau, P. Pianetta, C.M. Garner, C.Y. Su, and W.E. Spicer, Phys. Rev. B 18(1978) 5545.
14. N. Koshizaki, M. Kudo, M. Owari, Y. Nikei, and H. Kamada, Jpn. J. Appl. Phys. 19(1980) L349.
15. J.R. Lince and R.S.Williams, in Proceedings of the Conference on the Physics and Chemistry of Semiconductor Interfaces, in J. Vac. Sci. Technol. B 3(1985) xxx.

16. C.J. Cooke and W. Hume-Rothery, J. Less C. Metals 10(1966) 52.

17. R.T. Tung, J.M. Poate, J.C. Bean, J.M. Gibson, and D.C. Jacobson, Th. Sol. Films 93(1982) 77.

18. C.T. Tsai and R.S. Williams, to be published.

19. M.B.Panish, J. Electrochem Soc. 114(1967) 516.

20. M. Hansen, Constitution of Binary Alloys (McGraw-Hill, New York, 1958) p. 205

21. R. Ludeke, IBM J. Res. Develop. 22(1978) 304.

22. J.I. Goldstein, in Practical Scanning Electron Microscopy (Plenum, New York, 1975) pp. 81-87.

23. M.P. Seah and W.A. Dench, Surf. Interf. Anal. 1(1979) 2.

24. L.E. Davis, N.C. MacDonald, P.W. Palmberg, G.E. Riach, R.E. Weber, Handbook of Auger Electron Spectroscopy, 2nd ed. (Physical Electronics Div., Perkin-Elmer Corp., Eden Prairie, MN, 1978), p. 14.

25. J.R. Lince, J.G. Nelson, and R.S. Williams, J. Vac. Sci. Technol. B 1(1983) 553.

26. M.J. Lynch and J.B. Swan, Aust. J. Phys. 21(1968) 811.

27. M. Schluter, Z. Physik 250(1972) 87.

28. R.S. Williams, submitted to Th. Sol. Films.

29. C.H.P. Lupis, Chemical Thermodynamics of Materials (North-Holland, New York, 1983) Chap. I.

30. O. Kubaschewski and E.LL. Evans, Metallurgical Thermochemistry (Pergamon, London, 1958) Chaps. I, III.

31. B.D. Lichter and P. Sommelet, Trans. Met. Soc. AIME 245(1969) 1021.

32. B. Predel and D.W. Stein, Acta Met. 20(1972) 681.

33. J.H. Wernick, A. Menth, T.H. Geballe, G. Hull, and J.P. Maita,

J. Phys. Chem. Solids 30(1969) 1949.

34. G.N. Lewis and M. Randall, Thermodynamics (Mcgraw-Hill, New York, 1961) pp. 659-663.

35. R.E. Honig, RCA Review 23(1962) 567.

FIGURE CAPTIONS

Figure 1

SEM photographs of the annealed 496Å $AuGa_2$ film for (a) normal, and (b) 52° from normal electron beam incidence. They were both viewed with ~7000X magn, 20kV electron beam energy, and 100 μA electron beam current. The object in the upper right in (b) is a metallized dust particle.

Figure 2

AES spectra of the clean GaSb(001) surface, and of the 496Å $AuGa_2$ film on GaSb(001) before and after annealing to 747K. The Sb MNN doublet is at 454-462 eV, while the main Ga LMM peak is at 1070 eV. The Au 69 eV peak and the Au 239 eV peaks are shown expanded by 6X and 10X, respectively.

Figure 3

EELS spectra of (a) the annealed 3240Å $AuGa_2$ on GaSb(001), (b) the annealed 496Å $AuGa_2$ film on GaSb(001), and (c) spectra of the clean GaSb(001) surface at a primary electron energy of 300 eV. Assignments for the peaks are listed in Table I.

Figure 4

SEM photographs of the annealed 506Å Au on GaSb(001) film for (a) normal, and (b) 52° from normal electron beam incidence. They were both viewed with ~7000X magn., 20kV electron beam energy, and 100 μA electron beam current.

Figure 5

AES spectra of the clean GaSb(001) surface, and of the 506Å Au film on GaSb(001) before and after annealing to 723K. Peak assignments are in

the caption of Fig. 2.

Figure 6

EELS spectra of the 506Å Au film on GaSb(001) (b) before and (a) after annealing to 723K along with (c) spectra of the clean GaSb(001) surface for comparison. Primary electron energy was 300 eV. Some assignments for (b) are listed in Table I.

Figure 7

Plot of $(dN/dE)_{Ga}/(dN/dE)_{Sb}$ and $(dN/dE)_{Au}$ vs. progressively higher annealing temperature for a single sample of 40Å Au on GaSb(001). At the top of the Figure, the LEED patterns observed are shown. The AES peak-to-peak heights and LEED patterns were observed at RT.

a

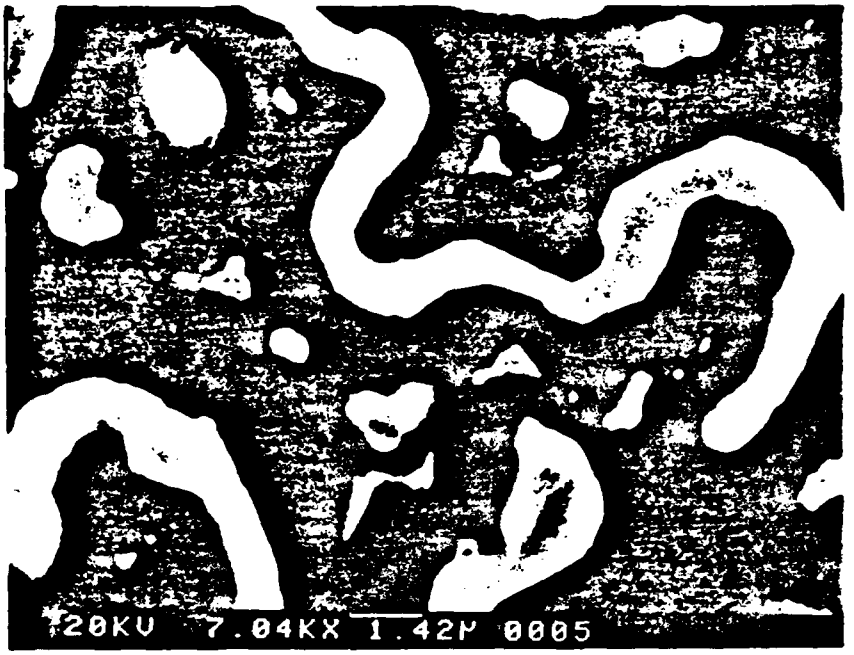

b

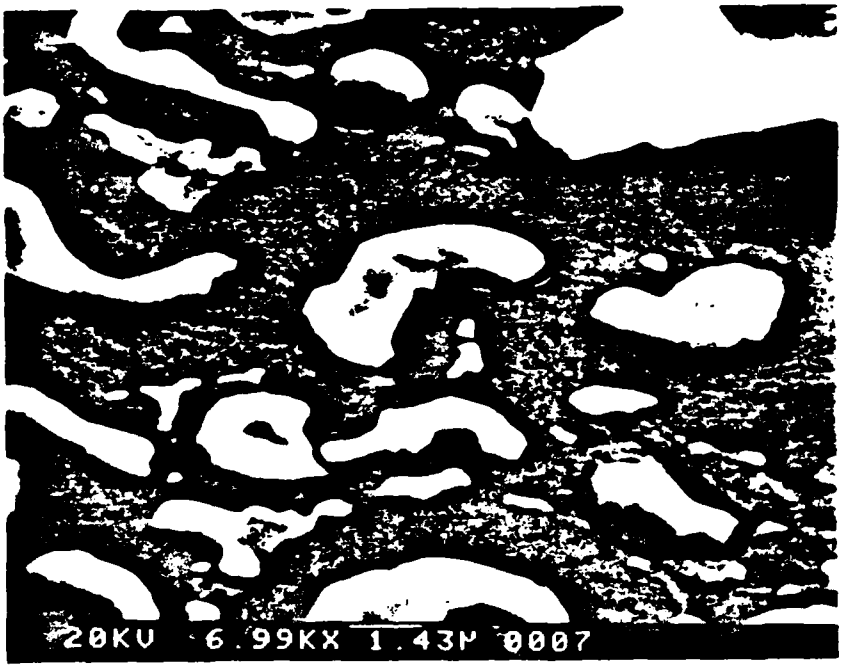

FIG. 1

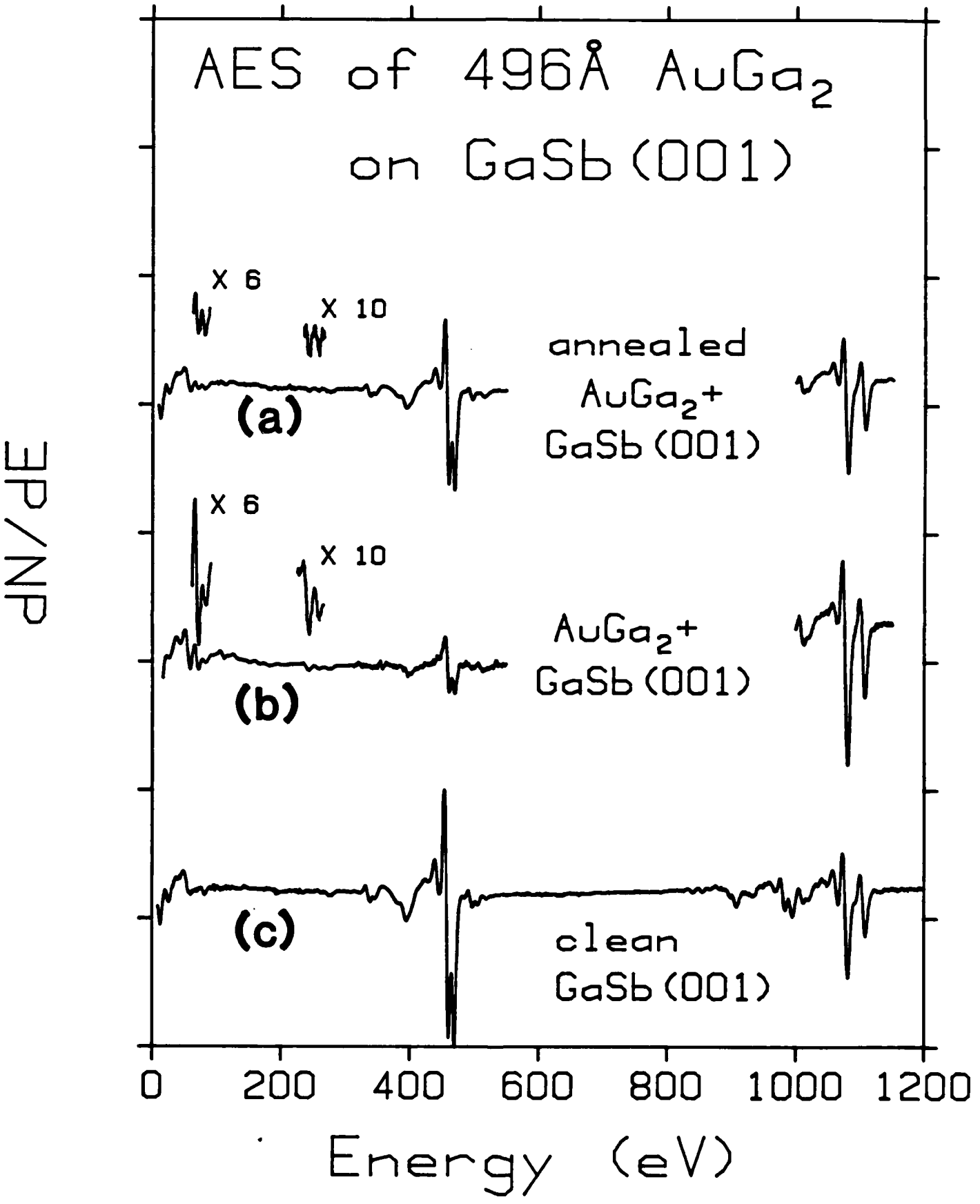
AES of 496Å AuGa2
on GaSb(001)
X 6
X 10
annealed
AuGa2+
GaSb(001)
(a)
X 6
X 10
AuGa2+
GaSb(001)
(b)
(c)
clean
GaSb(001)
dN/dE
0
200
400
600
800
1000
1200
Energy (eV)

FIG. 2

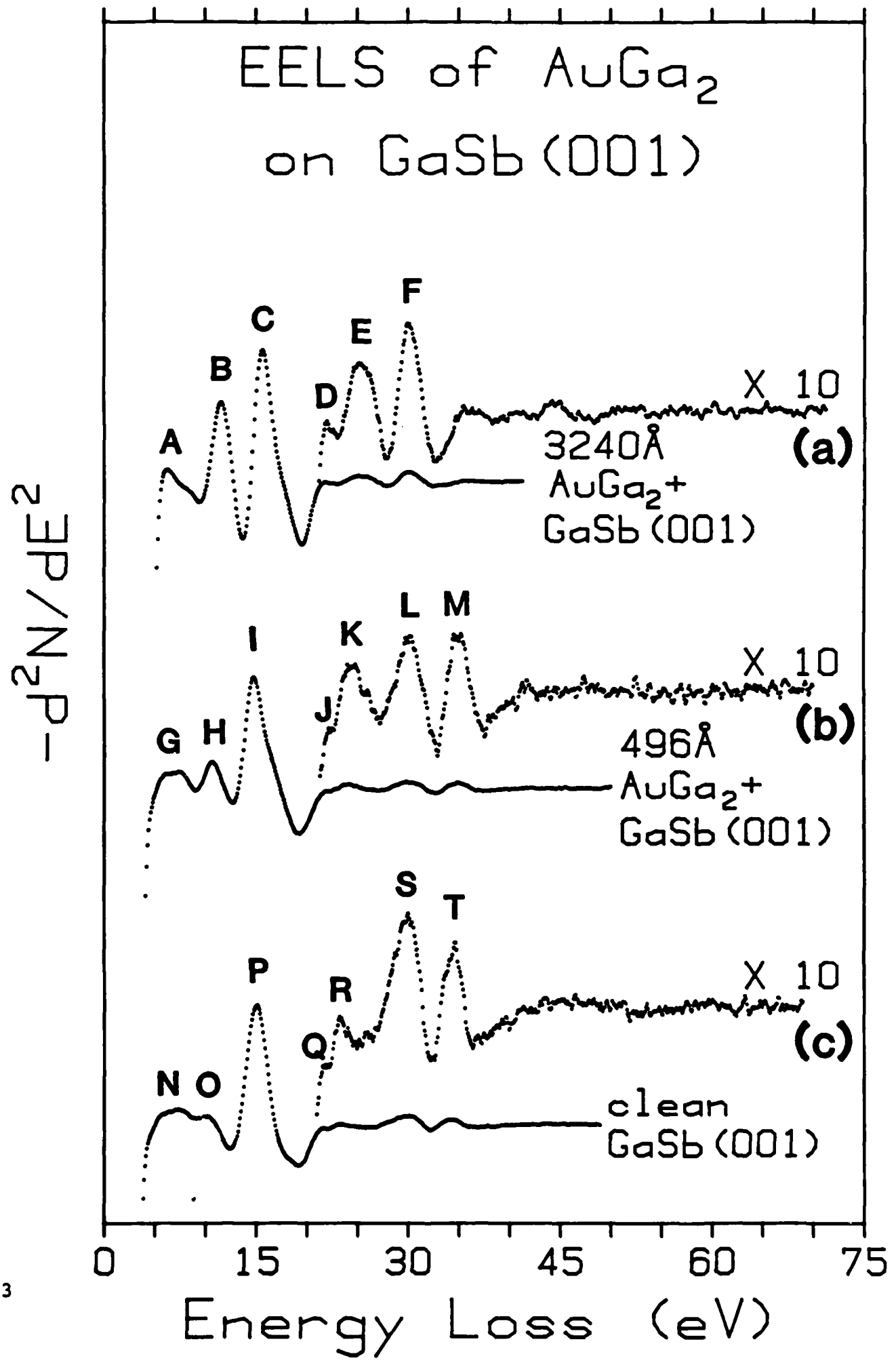
EELS of $AuGa_2$
on GaSb(001)
$-d^2N/dE^2$
A
B
C
D
E
F
X 10
3240Å
$AuGa_2$+
GaSb(001)
(a)
G
H
I
J
K
L
M
X 10
496Å
$AuGa_2$+
GaSb(001)
(b)
N
O
P
Q
R
S
T
X 10
clean
GaSb(001)
(c)
0
15
30
45
60
75
Energy Loss (eV)

FIG. 3

a

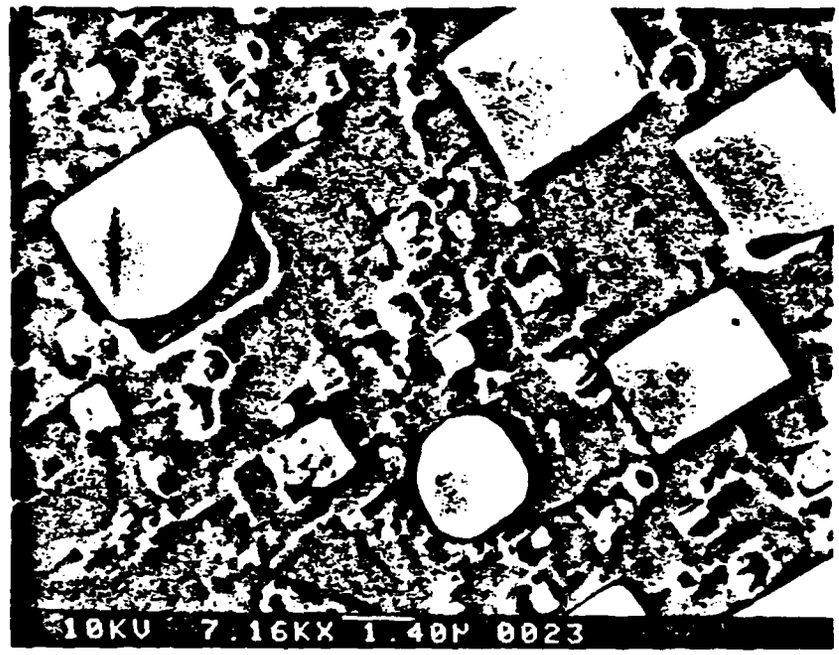

b

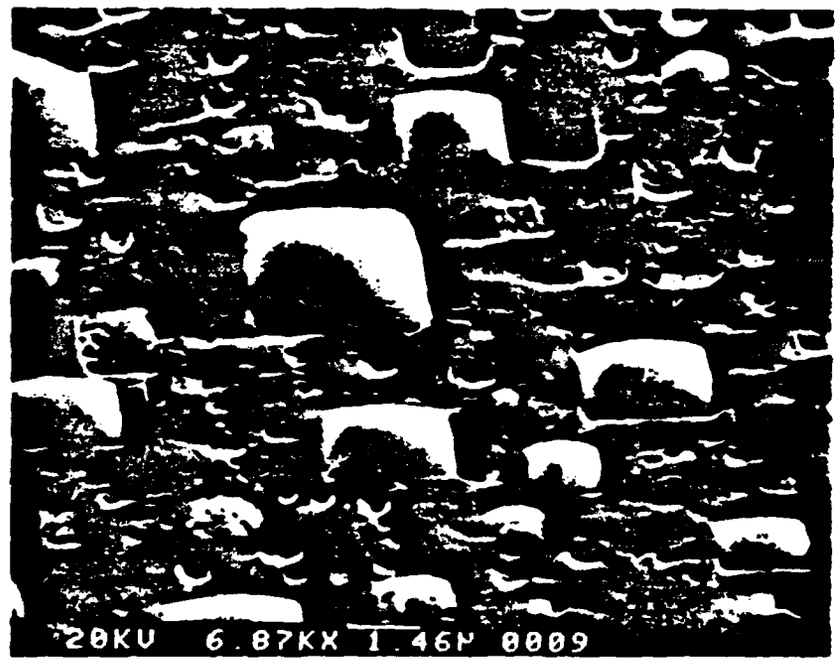

FIG. 4

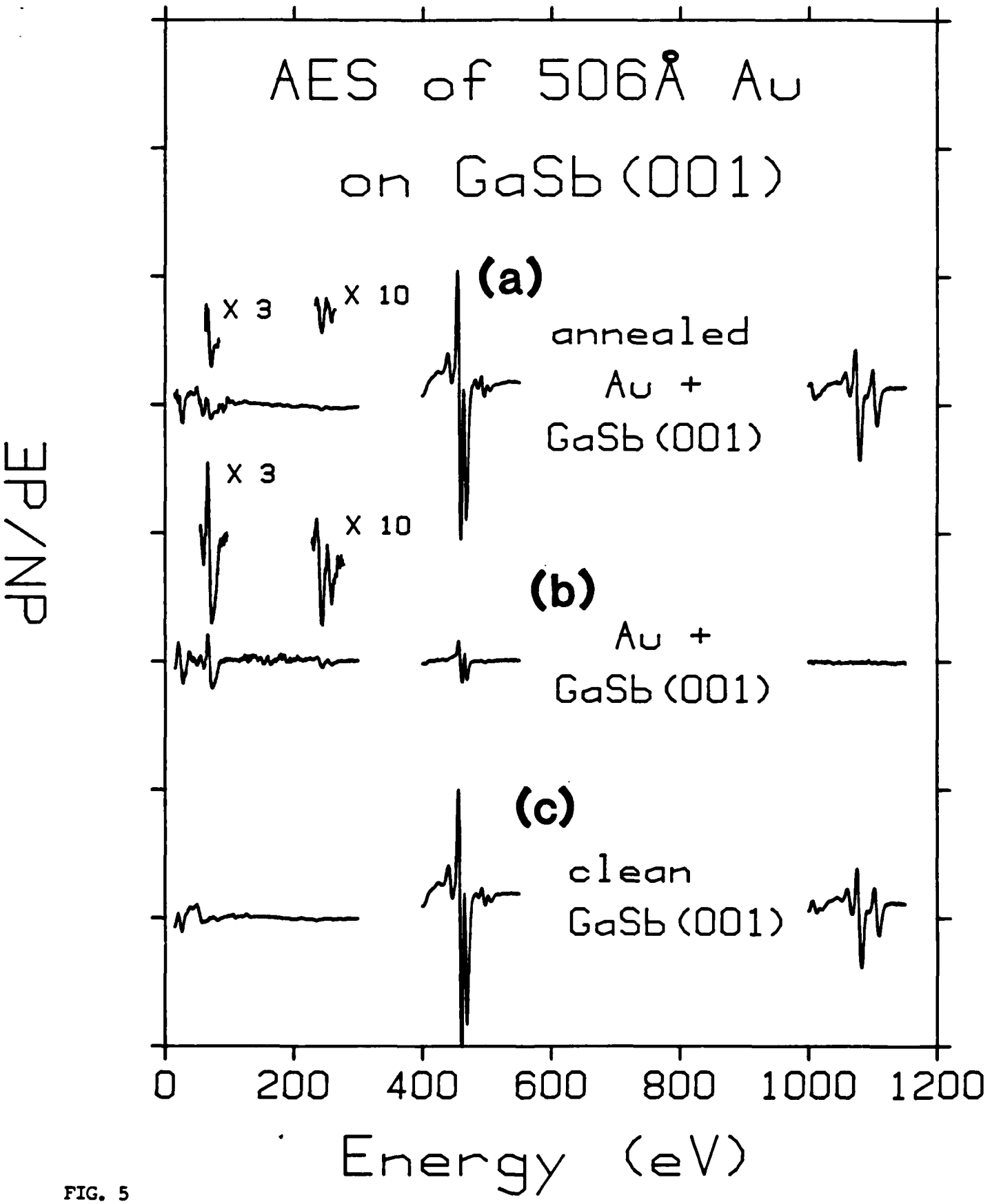
AES of 506Å Au
on GaSb(001)
(a)
X 3
X 10
annealed
Au +
GaSb(001)
X 3
X 10
(b)
Au +
GaSb(001)
(c)
clean
GaSb(001)
dN/dE
0
200
400
600
800
1000
1200
Energy (eV)

FIG. 5

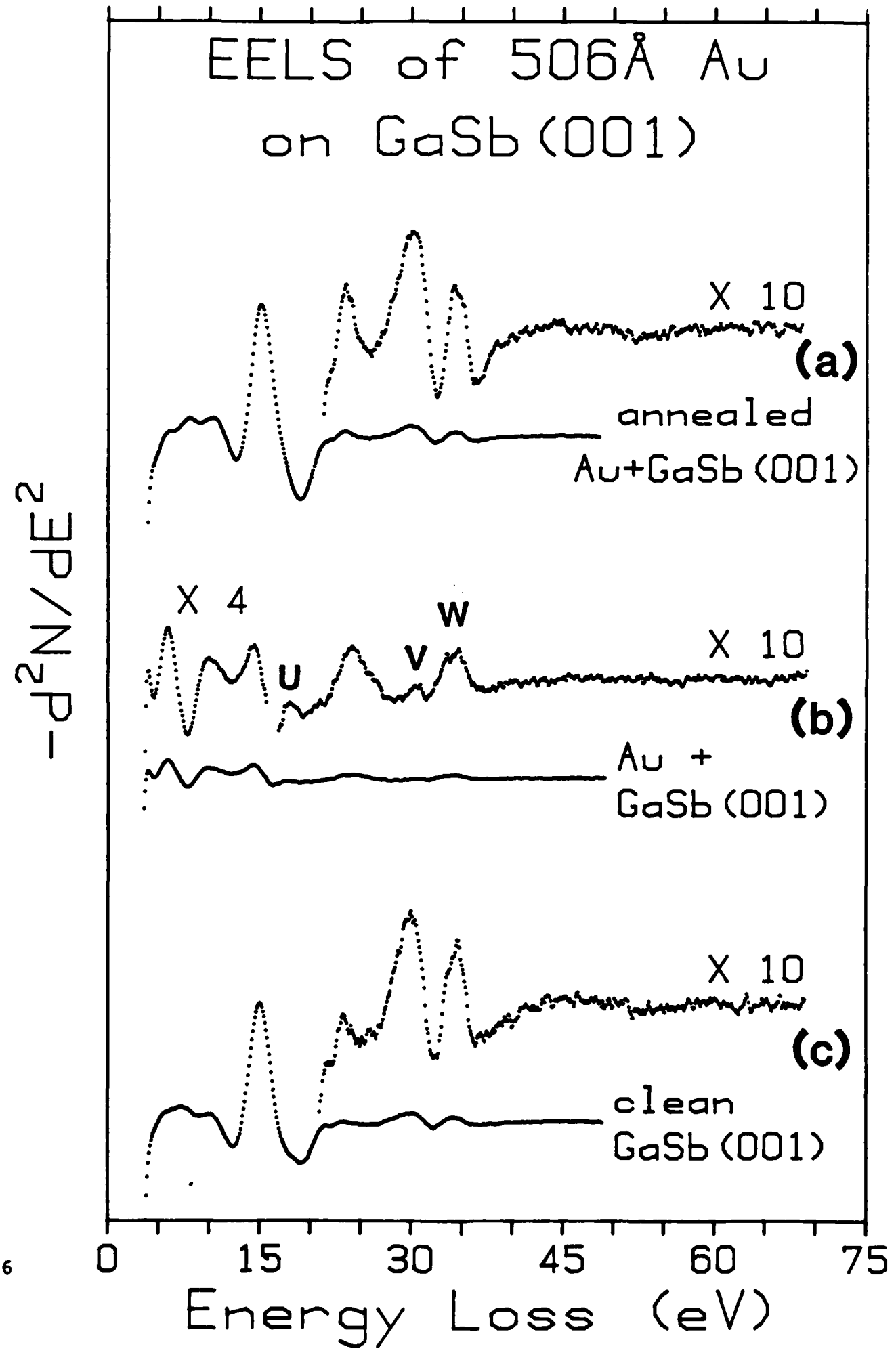
EELS of 506Å Au
on GaSb(001)
X 10
(a)
annealed
Au+GaSb(001)
X 4
W
X 10
U
V
(b)
Au +
GaSb(001)
X 10
(c)
clean
GaSb(001)
$-d^2N/dE^2$
0
15
30
45
60
75
Energy Loss (eV)

FIG. 6

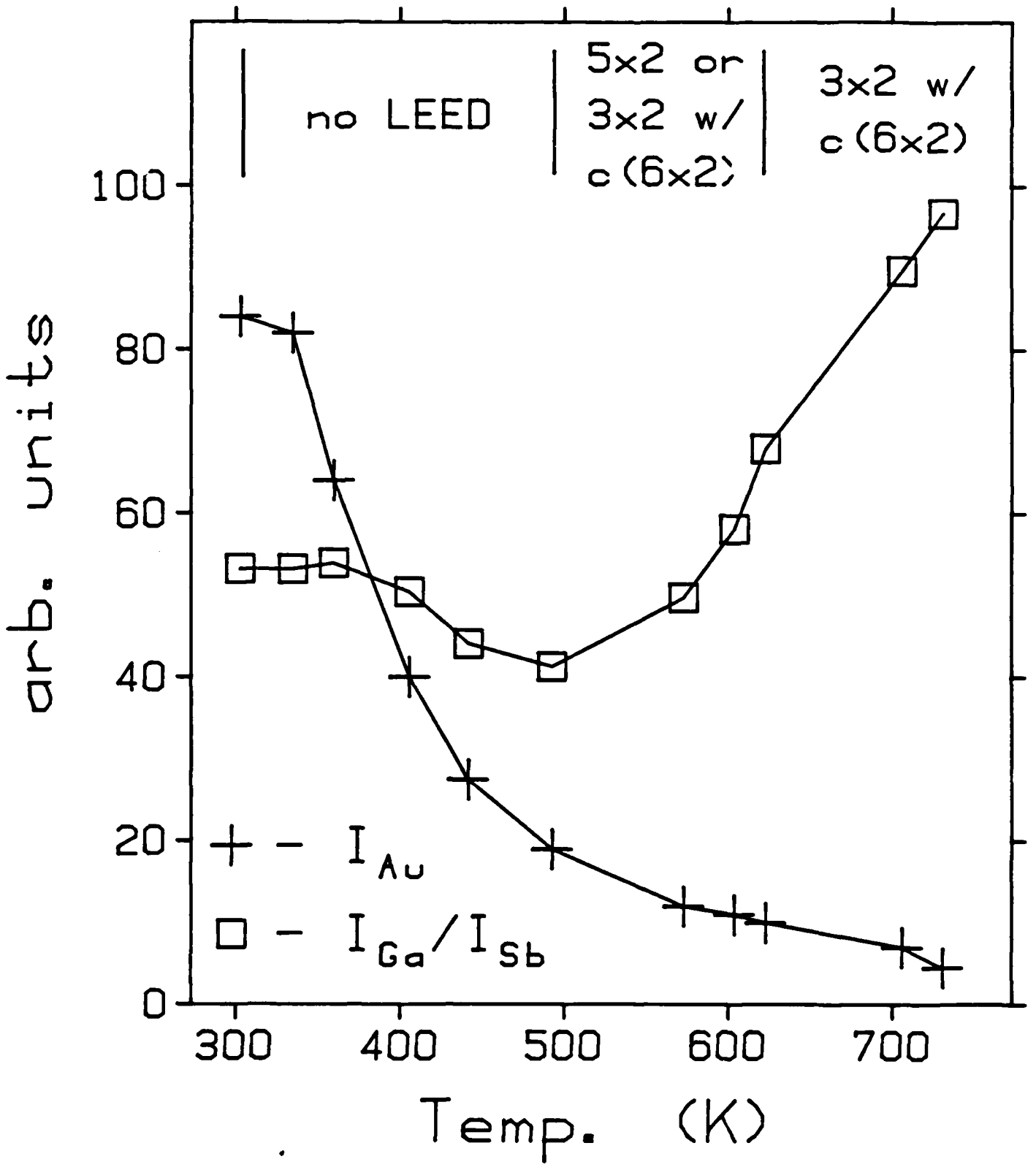
no LEED
5x2 or
3x2 w/
c(6x2)
3x2 w/
c(6x2)
100
80
60
40
20
0
arb. units
+ - I_{Au}
□ - I_{Ga}/I_{Sb}
300
400
500
600
700
Temp. (K)

FIG. 7

OFFICE OF NAVAL RESEARCH

Research Contract N00014-83-K-0612

TECHNICAL REPORT No. 9

HIGH-RESOLUTION ANGLE-RESOLVED PHOTOEMISSION STUDY OF THE Ag BAND STRUCTURE ALONG Λ

by

Jeffrey G. Nelson, Sehun Kim, W.J. Gignac and R. Stanley Williams

Department of Chemistry & Biochemistry
University of California, Los Angeles, CA 90024

and

J.G. Tobin, Steven W. Robey and D.A. Shirley

MMRD and Departments of Chemistry and Physics
University of California, Berkeley, CA 94720

To Be Published

in

Physical Review B

August 1985

PHYSICAL REVIEW B VOLUME 32, NUMBER 6 15 SEPTEMBER 1985

High-resolution angle-resolved photoemission study of the Ag band structure along Λ

Jeffrey G. Nelson,* Sehun Kim, W. J. Gignac,† and R. Stanley Williams
Department of Chemistry and Biochemistry, University of California, Los Angeles, California 90024

J. G. Tobin, Steven W. Robey, and D. A. Shirley
Materials and Molecular Research Division, Lawrence Berkeley Laboratory, University of California, Berkeley, California 94720 and Department of Chemistry and Department of Physics, University of California, Berkeley, California 94720
(Received 18 March 1985)

High-resolution angle-resolved photoelectron spectra have been obtained from the (111) face of an Ag crystal for normal electron emission. These spectra made it possible to determine experimentally the valence-band structure of Ag along the high-symmetry line Λ with better accuracy than previously [P. S. Wehner *et al.*, Phys. Rev. B 19, 6164 (1979)], and also revealed a second flat band near point Γ in the conduction bands 23 eV above the Fermi level. The new binding energies at points Γ and *L* were used along with the data of other workers to construct an experimental band structure of Ag with the mixed-basis interpolation scheme of Smith [Phys. Rev. B 9, 1365 (1974)]. The augmented-plane-wave calculations of Eckhardt, Fritsche, and Noffke [J. Phys. F 14, 97 (1984)] agree very well with the experimentally determined bands.
MS code no. BC3085 1985 PACS numbers: 71.25.Pi, 71.70.−d, 73.20.−r, 79.60.−i

I. INTRODUCTION

The bulk and surface electronic states of crystalline materials continue to be of great interest in the condensed-phase sciences. Angle-resolved photoelectron spectroscopy (ARPES) has become one of the primary techniques for investigating the band structure of solids.[1] Recent advances in the technology associated with photoelectron spectroscopy, such as intense continuum photon sources available at electron storage rings, high-resolution monochromators that can tune over a broad spectral region, and high-energy and momentum-resolution electron spectrometers, have made possible increasingly improved resolution in band-structure studies. This increase in resolutions has led to more accurate experimental determinations of energy-band dispersion relations, but it also requires a more careful examination of the assumptions involved in determining E versus $\mathbf{k}$ dispersion relations using ARPES data.

Assuming that some reasonable understanding of the photoelectron final state exists, ARPES spectra can be used as a direct probe of the dispersion relations of the initial states; i.e., the dependence of the valence-band binding energies upon the crystal momentum. For the case of photoelectron emission along the Ag[111] axis and the photon energy regime of this experiment, a particularly simple final-state band structure occurs. A single band, band 7 of the calculations of Christensen[2] and Eckhardt *et al.*,[3] is the only energetically accessible final state for photon energies up to 25 eV. This study presents results that are an extension of and improvement upon an earlier experiment,[4] which was performed with a larger photoelectron acceptance angle and poorer energy resolution. High-resolution ARPES data were collected at normal emission to the Ag(111) crystal face [$\mathbf{k}$ along the ΓΛL line in the three-dimensional Brillouin Zone (BZ)]. This improved resolution allowed the observation of previously undetected spectral features that were expected to occur from band-structure calculations.[2,3] A mixed-basis interpolation scheme, originally developed by Smith and coworkers,[5–7] was used to calculate an experimental band structure by fitting, according to a procedure discussed by Mattheiss,[8] to our measured values at points Γ and *L*, and to previously determined experimental energy values at points *X* and *K*.[9–15] The theoretical valence bands calculated by Eckhardt *et al.*[3] and the experimental data generally agreed to within 0.3 eV.

This paper is organized as follows. Section II contains the experimental details, Sec. III describes the photoemission results, Sec. IV is a discussion of the results and comparison with theory, and Sec. V presents a summary and final conclusions.

II. EXPERIMENTAL PROCEDURE

The experiment was performed at the Stanford Synchrotron Radiation Laboratory during dedicated running time on beam line 1-2, which has an effective photon range of 6–32 eV. The chamber was an ultrahigh-vacuum ARPES system that has been discussed in detail elsewhere.[16] During the experiment, the energy resolution of the photoelectron analyzer was set at 60 meV, and the half-angle acceptance was 3°. The total resolution was less than or equal to 100 meV for $6 \leq h\nu \leq 24$ eV, 110 meV for $h\nu = 26$ eV, 170 meV for $h\nu = 28$ eV, 190 meV for $h\nu = 30$ eV, and 210 meV for $h\nu = 32$ eV, all of these being full width at half maximum (FWHM) values, assuming that the analyzer and the monochromator contributions add in quadrature. At electron-beam currents near 35 mA in the storage ring and with $h\nu = 21$ eV, spectra typically required 20 min to collect, with maximum accumulated counts equal to 15 000 for a 0.039-eV-wide channel.

The sample was cleaned by continuous Ar-ion sputter-

ing during cycles of heating (15 min) and cooling (30 min). The experimental chamber was back-filled with 10^{-5}-torr Ar, and the maximum sample temperature during sputtering was approximately 600 °C. After sputtering, the sample was annealed to 400 °C for five minutes to ensure a well-ordered surface, as confirmed by low-energy electron diffraction (LEED) observations. Surface cleanness was checked by Auger-electron spectroscopy (AES), using the LEED optics as a retarding field analyzer. No sulfur or carbon were detected, but the carbon line was somewhat obscured by a silver Auger peak near 260 eV kinetic energy. The peak-to-peak Auger derivative signal ratios for $I_{O(510\,eV)}/I_{Ag(335\,eV)}$ was less than 0.005. Moreover, the presence and sharpness of the Ag(111) photoemission surface state confirmed the ordering and cleanness of the surface. The base pressure in the chamber was 8×10^{-10} torr after the cleaning procedure.

For the photoemission experiments, the crystal was aligned *in situ* by using laser light reflected from the sample and LEED. The sample was mounted such that the plane of incidence of the photon beam contained the sample normal ([111] axis), the polarization vector of the radiation (p polarized), and the [010] axis of the crystal. The angle of incidence of the light (θ_h) was 60° from the [111] axis.

III. RESULTS

The normal emission spectra taken with $h\nu=6-32$ eV are shown in Figs. 1–3, with the Fermi energy (E_F) used as the zero of the binding-energy (E_B) scale. Figure 1 contains the spectra taken at $h\nu=6-12$ eV. The peak near E_F, which has been identified as a surface state,[17] is very strong for these photon energies. The dispersion of the bulk band is obvious from the movement of the low E_B feature from $E_B=3.5$ eV at $h\nu=12$ eV to $E_B=1.5$ eV at $h\nu=7$ eV. It becomes increasingly difficult to assign the structures as they disperse into the inelastic electron tail. For example, there is a weak structure at $E_B=5$ eV in the $h\nu=11$ eV spectrum that could be a photoemission peak, but does not correspond to any state of the bulk band structure. In Fig. 2 ($h\nu=14-22$ eV), the features at $4.2\le E_B\le 7$ eV are associated with bands 1–6, and a leading shoulder is present at $E_B\le 4.2$ eV, for $h\nu\ge 16$ eV. The surface state near the Fermi edge is also apparent, particularly at the lower photon energies.

One of the most important features apparent in Fig. 3 ($h\nu=23-32$ eV) is the feature at a constant kinetic energy (E_k) of 17 eV (with respect to E_F). This peak can be seen in the ARPES spectra for $h\nu\ge 23$ eV, with an apparent $E_B=h\nu-17$ eV. The remaining features in Fig. 3, except for the leading shoulder at $E_B=4.3$ eV, can be attributed to direct transitions from the initial states, bands 1–6. The low E_B shoulder in these spectra has been assigned previously to the $3z^2-r^2$ state of the topmost Ag layer.[18] The excellent resolution allows weak features to

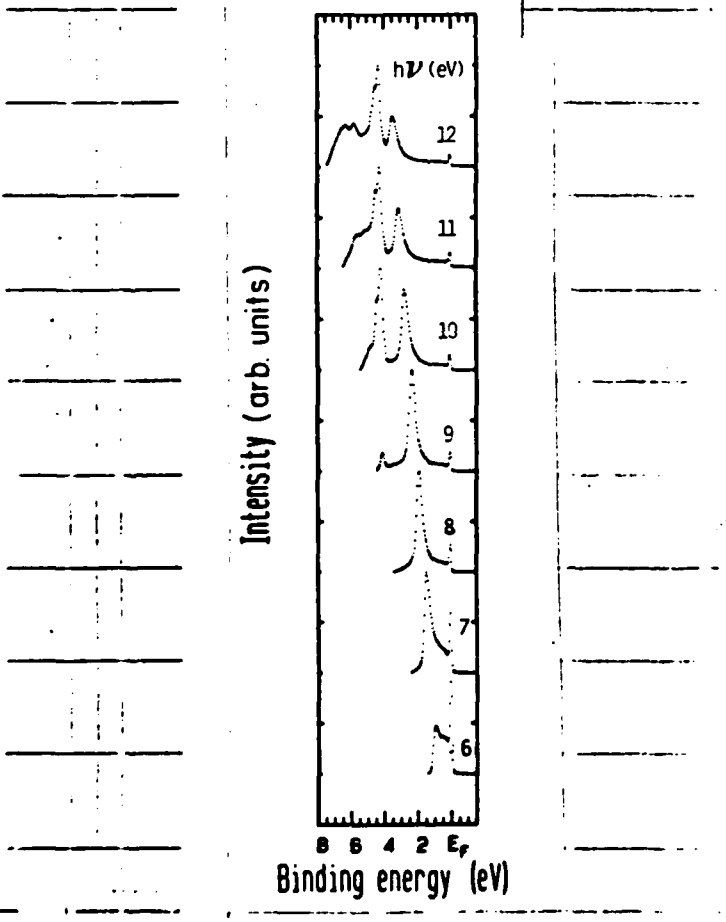

FIG. 1. ARPES EDC's for $h\nu=12$ (top); 11, 10, 9, 8, 7, and 6 eV (bottom) at normal emission.

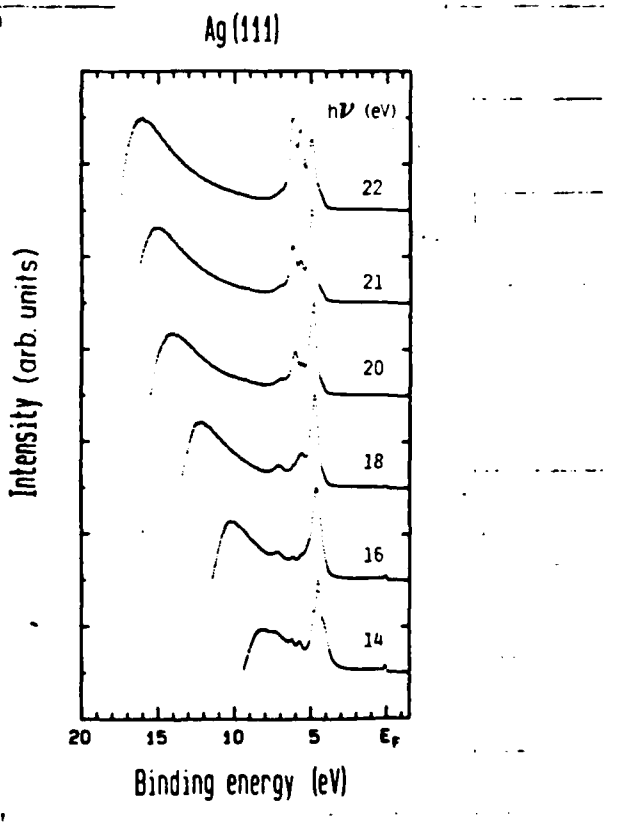

FIG. 2. ARPES EDC's for $h\nu=22$ (top); 21, 20, 18, 16, and 14 eV (bottom) at normal emission.

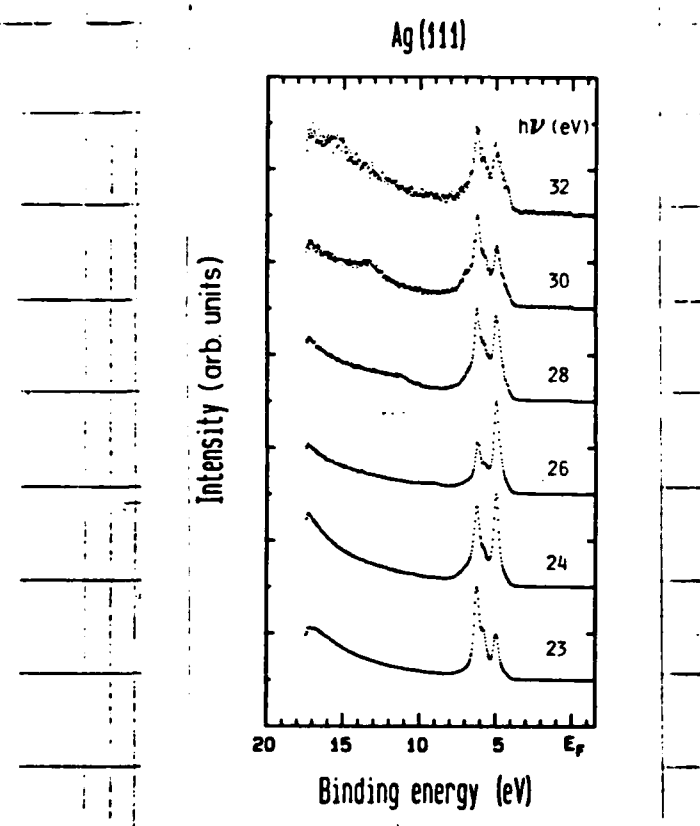

FIG. 3. ARPES EDC's for $h\nu=32$ (top); 30, 28, 26, 24, and 23 eV (bottom) at normal emission.

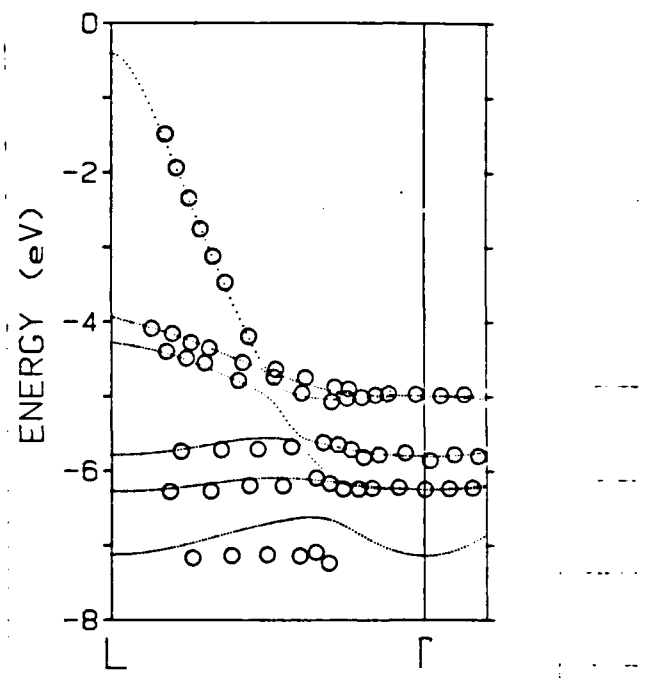

FIG. 4. Plot of valence-band binding energy with respect to E_F vs final-state wave vector for the normal emission results (open circles) and the interpolation scheme calculation (dotted lines).

be observed (especially in the spectra of Fig. 3) that were not evident in the previous study.[4]

IV. DISCUSSION

The experimentally determined parameters are the incident photon energy, the binding energy of the spectral features with respect to E_F, and the external exit angle of the photoelectrons with respect to the sample normal. If a knowledge of the final state exists, it is possible to work within the direct transition model[4] and determine the crystal momentum of the final and initial states.

In the case of Ag(111), the final state is reasonably well characterized for normal emission.[2-4] In order to map the photoemission peaks of Figs. 1–3 onto a band-structure plot, band 7 determined in Ref. 2 was fitted to a plane wave and used as a final state for the photoemission transitions. The final-state energy of a photoemission transition was determined by adding the appropriate photon energy to the binding energy of a peak in one of the spectra. The **k** value of the final state, and thus also of the initial state, was determined by the plane-wave dispersion relation. Since the dispersion of a plane-wave final-state band is so steep, a 1-eV shift of the final-state band corresponds to a change in the **k** value of only 5% of the interval from point Γ to point L. Thus, the determination of the initial-state band structure is only weakly dependent upon the final-state band chosen as a reference. The experimental bands (open circles in Fig. 4) were then plotted as the binding energy of the photoemission peaks referenced to E_F versus the value of **k** determined above.

The spectra of Figs. 1–3 also indirectly provide information about the actual final-state bands in Ag. The feature that appears at a constant E_k of 17 eV has been discussed previously.[4] It is the result of a flattening of the final-state band, which carries the secondary electron current in the [111] direction to the analyzer, near point Γ. The effect of this flat-band region may also be seen in the intensities of the peaks in the ARPES spectra for photon energies from 21 to 24 eV. As the photon energy is varied, transitions from different valence bands are connected to the flat-band region at 17 eV above E_F, and sharp intensity increases are observed for peaks corresponding to the different initial states in the photoemission spectra because of the high density of final states. However, one observes a similar trend in the peak intensities of the spectra for photon energies from 26 to 30 eV, which implies that there is another flat-band region in the conduction bands at ~23 eV above E_F near point Γ. There are two pieces of evidence to support this hypothesis. First, there are striking similarities between the pairs of spectra $h\nu=20$ and 26, $h\nu=22$ and 28, $h\nu=24$ and 30, and $h\nu=26$ and 32 eV in Figs. 2 and 3. The degraded resolution at $h\nu\geq 26$ eV has the effect of smearing out some of the features but the resemblance is still strong. Second, in the $h\nu=32$ eV spectrum a very weak feature is seen at 9 eV apparent E_B, and at $h\nu=30$ eV there is an extra shoulder at 7 eV. This feature appears to have a constant E_k given by $E_B=h\nu-23$ eV, which would correspond to a flat final-state band 23 eV above E_F. The effect of these two flat-band regions is to create a band gap that is 6 eV wide with boundaries at 17 and 23 eV above E_F.

Also shown in Fig. 4 are the results of a mixed-basis interpolation scheme calculation. This computational method was first utilized by Smith *et al.*[5–7] to calculate the band structure of transition metals. The Ag parameters determined by Benbow and Smith[7] were used as starting values and were then adjusted using a nonlinear least-squares routine[8] to fit the interpolated bands to 22 experimental energy values at the Γ, L, X, and K symmetry points of the BZ determined here and in previous studies.[9–15] Table I shows a list of Ag energy bands at selected symmetry points. The values listed as experimental energies are all the band energies at symmetry points determined in this study and found in the literature. The values used in the least-squares fitting procedure are those farthest to the left in any particular row. Since this study did not access the L point of the BZ directly, the L-point binding energies listed in Table I were obtained by extrapolating the experimentally determined bands to the L point, using the calculations of Ref. 3 as a guide. Because the highest binding-energy photoemission feature in the spectra did not disperse, it was assumed that photoemission from the most tightly bound band was dominated by indirect transitions[19] originating near the L point, where the d-orbital character of the band, and thus its photoemission cross section, are the greatest.

The results of our interpolation scheme calculation, as

TABLE I. Energy values of Ag at selected symmetry points.

Symmetry label	Experimental energies[a]				Interpolation scheme energies	Theoretical energies[b]
Γ_6^+ [c]					−7.13	−7.21
Γ_8^+	−6.23[d]	−5.92[e]	−6.15[f]	−6.16[g]	−6.24	−5.82
Γ_7^+	−5.80[d]	−5.48[e]	−5.50[f]	−5.64[g]	−5.80	−5.37
Γ_8^+	−4.95[d]	−4.78[e]		−5.00[g]	−4.98	−4.69
Γ_7^-	+17.0[d]	+17.0[e]	17.1[h]		17.18	17.01
Γ_6^-,Γ_8^-	+23.0[d]				23.0	19.93
L_6^+	−7.13[d]	−6.94[e]			−7.12	−6.74
L_4^+,L_5^+	−6.28[d]	−5.82[e]			−6.27	−5.91
L_6^+	−5.74[d]	−5.53[e]			−5.78	−5.44
L_6^+	−4.31[d]	−4.20[e]			−4.28	−4.23
L_4^+,L_5^+	−4.06[d]	−3.96[e]	−3.99[i]		−3.94	−4.01
L_6^-		−0.30[e]	−0.31[i]	−0.31[j]	−0.40	−0.03
L_6^+	+3.77[k]	+3.85[l]		+3.86[j]	+3.84	+3.36
X_6^+	−7.35[f]	−7.30[g]			−7.36	−7.00
X_7^+	−7.00[f]				−7.01	−6.82
X_7^+	−4.20[f]	−4.36[g]			−4.26	−4.25
X_6^+		−4.12[g]			−4.16	−4.05
X_7^+	−3.90[f]	−3.82[g]			−3.82	−3.71
X_6^-		+2.10[k]			+1.90	+2.05
K_1^+	−7.00[f]				−6.93	−6.62
K_1^+ [c]					−6.48	−6.16
K_3^+	−5.28[f]				−5.26	−4.96
K_4^+	−4.70[f]				−4.75	−4.58
K_2^+	−4.28[f]				−4.38	−4.13

[a] All energies with respect to the Fermi energy in units of eV.
[b] Reference 3.
[c] No experimental determinations of these points exist.
[d] This work.
[e] Reference 4.
[f] Reference 10.
[g] Reference 11.
[h] Reference 15.
[i] Reference 13.
[j] Reference 9.
[k] Reference 12.
[l] Reference 14.

well as those of the *ab initio* calculation of Eckhardt *et al.*,[3] are given in the last two columns. The agreement between the interpolation scheme calculation and the chosen experimental values is excellent, with only a 0.1-eV rms deviation over the 22 **k** points used in the fit. Table II lists the parameters determined by the fitting procedure, along with those reported in Ref. 7. The interpolation scheme was used to calculate the Ag bands, which are shown as dotted lines in Fig. 4, along the Λ line. Even though the interpolation scheme was fit to values only at symmetry points, the agreement between the experimental and interpolated bands is excellent all across the Λ line. Furthermore, the agreement of the theoretical bands[3] with the experimental values is also very good. Excluding the $+23$ eV conduction band at Γ, the rms deviation of the experimental and theoretical bands at the **k** points listed in Table I is 0.28 eV, and decreases to 0.21 eV if the theoretical bands are shifted downward by 0.17 eV. These differences are not much larger than the experimental resolution of the measurements.

One curious result is that the interpolation scheme yields nearly equal energies for the Γ_6^+ and the L_6^+ points of the BZ. Since no experimental value was available for the Γ_6^+ point, an initial fit to the experimental energies neglected this point and produced a band structure very similar to that reported here, except that the energy of the Γ_6^+ point was -6.95 eV, which is higher in energy than the L_6^+ point. The present band structure was obtained by artificially fitting the energy of the Γ_6^+ point to a value of -7.4 eV. Attempts to lower the energy of the Γ_6^+ band further began to disrupt seriously the agreement of the calculations with the experimentally determined energy eigenvalues.

The interpolation scheme calculation was extended to higher energies in order to look at the band gap 17–23 eV above point Γ. Figure 5 shows the conduction bands to 30 eV above E_F, in addition to the previously discussed valence bands. Although the existence of the gap does not appear to inhibit photoemission in the gap region, its existence could be inferred indirectly from the features of constant kinetic energy in the photoemission spectra. The existence of the flat band at 17 eV is supported quantitatively by a sharp peak in the low-energy-electron reflectance spectrum of Ag(111) reported by Jaklevic and Davis.[15] The reflectance spectrum also reveals a shoulder near 23 eV, but a definite assignment of this feature is not possible. In any case, the band gap appears, from the reflectance data, to be fairly wide.

Indirect transitions have been invoked to explain the broad *sp* plateau observed in ARPES spectra from Ag(111).[4] If the indirect transitions are caused by thermal broadening around a direct transition in **k** space, the region of the BZ contributing to transitions into a final state will be limited, and variations of the photoemission intensity arising from indirect transitions will occur as the wave vector is varied. Figure 6 shows a plot from this experiment of the ratio of the *sp*-plateau height to the valence-band integrated intensity and to the maximum intensity of the valence band. Both the plots show similar results: the minima in both ratios are at $h\nu=25$ eV, and the ratios increase rapidly to both higher and lower pho-

TABLE II. Parameters used in interpolation scheme calculation of the Ag band structure.

Parameter[a,b]	Value (eV)	Standard deviation (eV)	Previous[c] value (eV)
E_0	1.94	0.37	1.46
Δ	−0.076	0.72	−0.053
A_1	0.007	0.16	0.15
A_2	−0.034	0.11	0.029
A_3	0.008	0.18	0.074
A_4	0.052	0.18	0.090
A_5	0.018	0.13	0.022
A_6	0.051	0.15	0.060
S	2.18	5.93	20.1
B_1	25.1	3.59	19.6
B_2	24.5	5.47	19.6
α	0.157	0.003	0.14
R	0.27	0.04	0.29
V_{000}	−0.45	0.41	−0.51
V_{111}	1.38	0.39	0.85
V_{200}	1.60	0.28	0.66
V_{220}	−0.014	(2)	−0.014
V_{311}	1.15	(2)	1.15
V_{222}	1.69	(2)	1.69
ξ	0.258	(2)	0.26
E_F	6.04	(2)	6.04

[a] For definitions of the parameters, see Ref. 5.
[b] These parameters were not varied.
[c] These are the values for Ag reported by Benbow and Smith, Ref. 7.

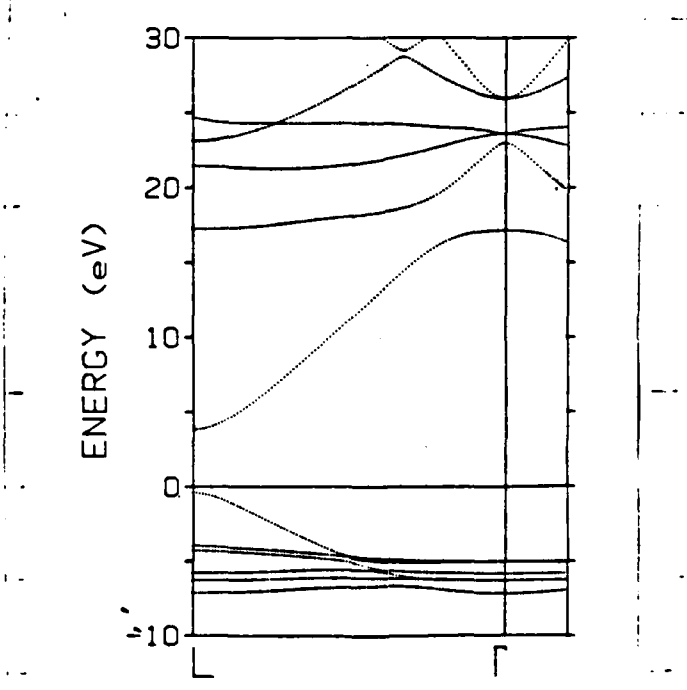

FIG. 5. Interpolation scheme calculation results showing conduction bands to 30 eV above the Fermi level. Flat-band regions 17 and 23 eV above E_F at Γ, discussed in Sec. IV, are shown.

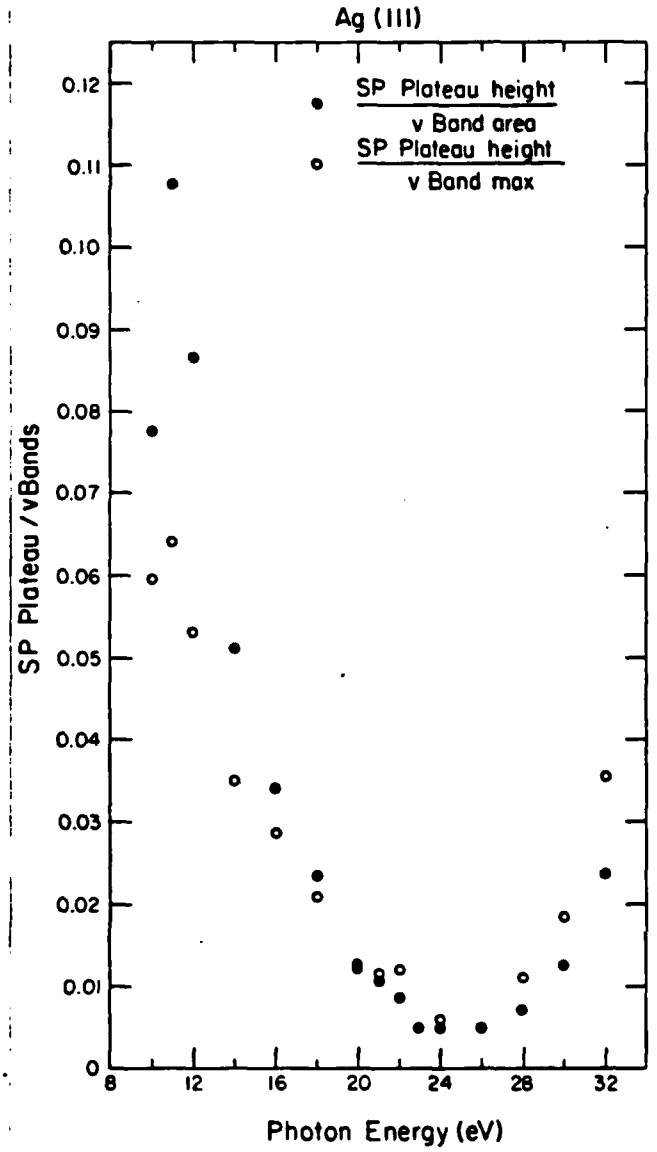

FIG. 6. Ratio of the *s-p* plateau height to the valence-band integrated intensity (solid circles) and to the maximum intensity of the valence band (open circles) vs photon energy.

ton energies. The minima correspond to transitions originating near point Γ, and the intensity increases as the final-state wave vector moves toward point *L* in either direction. This increase in intensity is due to contributions from band 6 and other valence bands as the region of the BZ sampled by the indirect transitions moves away from point Γ towards point *L*. Similar effects are observed in ARPES spectra from all three of the lowest-Miller-index surfaces of Cu.[18]

V. SUMMARY

Improved energy- and angular-resolution ARPES data have revealed previously unobserved bulk photoemission features from the Ag(111) surface. Experimental determination of the Ag band structure was expanded and of improved accuracy. A mixed-basis interpolation scheme was fit to the experimentally determined bands at several symmetry points in the BZ. The bands calculated using the interpolation scheme agree very well with the photoemission results all along the high-symmetry line Λ of the BZ, and also with the first-principle calculations of Eckhardt *et al.*[3] The existence of a 6-eV band gap in the conductions bands 17–23 eV above the Fermi level at point Γ of the BZ was also inferred from the photoemission data. Finally, the intensity of the "*s-p* plateau" just below E_F in the photoemission spectra was shown to be a minimum for photoelectron transitions near the Γ point.

ACKNOWLEDGMENTS

This work was performed at the Stanford Synchrotron Radiation Laboratory, which is supported by the U. S. Department of Energy under Grant No. DE-AC03-82ER13000, in cooperation with the Stanford Linear Accelerator Center. Support for this project was provided by the U.S. Office of Naval Research, Department of the Navy and by the Division of Chemical Sciences, Office of Basic Energy Sciences, U.S. Department of Energy under Contract No. DE-AC03-76SF00098. R.S.W. acknowledges the Camille and Henry Dreyfus Foundation and the Alfred P. Sloan Foundation for support. J.G.T. was supported in part by the National Science Foundation.

*Present address: Rockwell Science Center, 1049 Camino Dos Rios, Thousand Oaks, CA 91360.
†Present address: Hughes Research Laboratories, 3011 Malibu Canyon Road, Malibu, CA 90265.
‡Present address: Department of Chemistry, University of Wisconsin, Madison, WI 53706.

[1]R. H. Williams, G. P. Srivastava, and I. T. McGovern, Rep. Prog. Phys. 43, 1357 (1980).
[2]N. E. Christensen, Phys. Status Solidi B 54, 551 (1972).
[3]H. Eckhardt, L. Fitsche, and J. Noffke, J. Phys. F 14, 97 (1984).
[4]P. S. Wehner, R. S. Williams, S. P. Kevan, D. Denley, and D. A. Shirley, Phys. Rev. B 19, 6164 (1979).
[5]N. V. Smith and L. F. Mattheiss, Phys. Rev. B 9, 1341 (1974).
[6]N. V. Smith, Phys. Rev. B 9, 1365 (1974).
[7]R. L. Benbow and N. V. Smith, Phys. Rev. B 27, 3144 (1983).
[8]L. F. Mattheiss, Phys. Rev. B 5, 290 (1972).
[9]L. Wallden and T. Gustafsson, Phys. Scr. 6, 73 (1972).
[10]K. A. Mills, Ph.D. thesis, University of California, LBL Report No. 9429, 1979 (unpublished).
[11]R. Courths, V. Bachelier, and S. Hufner, Solid State Commun. 38, 887 (1981).
[12]B. Reihl and R. R. Schittler, Phys. Rev. B 29, 2267 (1984).
[13]R. Rosei, C. H. Culp, and J. H. Weaver, Phys. Rev. B 10, 484 (1974).
[14]C. E. Morris and D. W. Lynch, Phys. Rev. 182, 719 (1969).
[15]R. C. Jaklevic and L. C. Davis, Phys. Rev. B 26, 5391 (1982).
[16]S. D. Kevan and D. A. Shirley, Phys. Rev. B 22, 524 (1980); S. D. Kevan, Ph.D. thesis, University of California (1980).
[17]H. F. Roloff and H. Neddermeyer, Solid State Commun. 21,

561 (1977); P. Heimann, H. Neddermeyer, and H. F. Roloff, J. Phys. C 10, L17 (1977).
[18]J. G. Tobin, Ph.D. thesis, University of California, (1983); J. G. Tobin, S. W. Robey, L. E. Klebanoff, and D. A. Shirley, Phys. Rev. B 28, 6169 (1983).
[19]R. S. Williams, P. S. Wehner, J. Stohr, and D. A. Shirley, Phys. Rev. Lett. 39, 302 (1977).

SECURITY CLASSIFICATION OF THIS PAGE (When Data Entered)

REPORT DOCUMENTATION PAGE		READ INSTRUCTIONS BEFORE COMPLETING FORM
1. REPORT NUMBER 9	2. GOVT ACCESSION NO.	3. RECIPIENT'S CATALOG NUMBER
4. TITLE (and Subtitle) HIGH-RESOLUTION ANGLE-RESOLVED PHOTOEMISSION STUDY OF THE Ag BAND STRUCTURE ALONG Λ.		5. TYPE OF REPORT & PERIOD COVERED Technical Report - Dec 84-Aug 85 6. PERFORMING ORG. REPORT NUMBER
7. AUTHOR(s) Jeffrey G. Nelson, Sehun Kim. W.J. Gignac and R. Stanley Williams		8. CONTRACT OR GRANT NUMBER(s) N00014-83-K-0612
9. PERFORMING ORGANIZATION NAME AND ADDRESS UCLA Los Angeles, CA 90024		10. PROGRAM ELEMENT, PROJECT, TASK AREA & WORK UNIT NUMBERS
11. CONTROLLING OFFICE NAME AND ADDRESS Chemistry Program Office Office of Naval Research, Arlington VA 22217		12. REPORT DATE August 1985 13. NUMBER OF PAGES 25
14. MONITORING AGENCY NAME & ADDRESS(if different from Controlling Office)		15. SECURITY CLASS. (of this report) UNCLASSIFIED 15a. DECLASSIFICATION DOWNGRADING SCHEDULE

16. DISTRIBUTION STATEMENT (of this Report)

Approved for public release; distribution unlimited

17. DISTRIBUTION STATEMENT (of the abstract entered in Block 20, if different from Report)

18. SUPPLEMENTARY NOTES

To be published in Physical Review B (1985)

19. KEY WORDS (Continue on reverse side if necessary and identify by block number)

Ag(111) — band structure -- angle-resolved photoemission

20. ABSTRACT (Continue on reverse side if necessary and identify by block number)

High-resolution angle-resolved photoelectron spectra have been obtained from the (111) face of an Ag crystal for normal electron emission. These spectra made it possible to determine experimentally the valence band structure of Ag along Λ with better accuracy than previously, and also revealed a second flat band near Γ in the conduction bands 23 eV above the Fermi level. The new binding energies at Γ and L were used along with the data of other workers to construct an experimental band structure of Ag with the mixed basis interpolation

/MORE/

scheme of Smith. The APW calculations of Eckhardt, Fritche, and Noffke agree very well with the experimentally determined bands.

END

FILMED

10-85

DTIC